Finite Rate Innovation and its applications in Electrocardiography

Amrish Nair

SCHOOL OF ELECTRICAL & ELECTRONIC ENGINEERING

This thesis is submitted to Nanyang Technological University
in partial fulfillment of the requirement for the degree of
Master of Engineering

2015

Acknowledgements

Firstly, I would like to dedicate this to my wife, Shanthini, and my parents, Papa and Mummy. I know being a graduate student does not count as a real job. You have held my hand, been my rock, and now it is my turn to repay this immeasurable debt. I would like to thank Qualcomm Inc., and in particular, Frank Quick, Ronald Crochiere, James Determan and Jess Dominguez for their technical guidance and mentoring. I would also like to thank Adj Prof David Foo from Tan Tock Seng Hospital for the medical collaboration and valuable advice. To Talal and Sam, our regular afternoon coffees were both illuminating academically as they were enjoyable and I look forward to working with you again soon. To Nikhil ,Lavanya, Tian Jin, Srini, Gaetano, Andreas and Rehka, your friendship and time in the lab will not be forgotten. Finally I would like to thank Associate Professor Pina Marziliano without whose support and mentorship this work would not have been possible.

Contents

Acknowledgements **iii**

Abstract **ix**

Acronyms **xi**

List of Figures **xii**

List of Tables **xv**

1 Introduction **3**

2 Background **9**

2.1 Electrocardiography 9

2.2 Finite Rate of Innovation 12

2.3 VPW-FRI 15

2.4 Sparse sampling in ECG 18

2.4.1 FRI in ECG: ECG as splines 18
2.4.2 VPW-FRI in ECG: ECG as pulses 20
2.5 Data 22
2.5.1 TTSH Data Set 23
2.5.2 NTU Data Set 23

3 Multichannel ECG Analysis using the Common Annihilator 25
3.1 Common Annihilator Method 26
3.2 Results 28
3.3 Discussion 29

4 Order Estimation of VPW-FRI pulses applied to ECG 35
4.1 Background 35
4.2 Second Order Differential Method 36
4.3 Results 38
4.4 Conclusion and Future Work 44

5 Wave Detection in ECG 45
5.1 Background 45
5.2 R Peak Detection 46
5.2.1 Method 46
5.2.2 Results 47

5.3 Fetal R Peak Detection 48
5.3.1 Method 50
5.3.2 Results 53
5.4 P and T Wave Detection with Gaussian Kernel 55
5.4.1 Method 56
5.4.2 Results 60
5.5 Discussion 62

6 Conclusion and Future Work **65**

List of Publications **67**

Abstract

Compression and reconstruction of Electrocardiograms (ECG) has been a common topic of research in signal processing as wavelets, compressed sensing and many other methods have been used. However, the goal of this thesis was to demonstrate a sampling scheme, Variable Pulse Width Finite Rate of Innovation (VPW-FRI), whose samples provided meaningful information. The samples could be split into subspaces which were associated to the different waveforms in an ECG and hence specific features could be reconstructed directly from the samples without having to reconstruct the entire signal. This allowed for many clinical applications such as heart rate determination, fetal heart rate calculation and P and T wave detection. This extended to a multichannel sampling scheme. Since this is a subspace method, it had robust de-noising capabilities. The novel subspace method developed in this thesis solves many of the earlier limitations of VPW-FRI and FRI and the efficacy will be demonstrated on data from hospitals and medical devices.

Acronyms

ECG	Electrocardiogram
FRI	Finite Rate of Innovation
VPW-FRI	Variable Pulse Width Finite Rate of Innovation
SVD	Singular Value Decomposition
SNR	Signal to Noise Ratio
CR	Compression Ratio
HR	Heart rate

List of Figures

2.1 ECG waveform and its constituent waves 10

2.2 Lead placement for ECG. Three lead ECG uses leads LA, RA, LL and RL whereas the twelve lead ECG uses all the leads including V1-6. 12

2.3 Symmetric and asymmetric components of a VPW-FRI pulse . 16

3.1 Reconstruction of 12 lead ECG from Data Set A. 31

3.2 Compression ratio of VPW-FRI vs Heart Rate 32

3.3 De-noising of an ECG heart beat with added AWGN $10dB$. . 32

3.4 Comparison of modeling accuracy using single lead and multichannel ECG 33

4.1 Singular Values vs Second Order Difference 37

4.2 Reconstruction of Lead 2 using $K = 10$ 38

4.3 Singular values with Order Estimation 39

4.4 Mean and standard deviation of SRR for different values of K 39

4.5 Reconstruction of Lead 2 with AWGN at 10dB 40

4.6 Comparison of second order difference of clean ECG signal and the same segment with 5dB of AWGN 43

4.7 Reconstruction of noisy ECG with $K = 8$ 43

5.1 R peak detection on an ECG signal with AWGN $0dB$ 48

5.2 Singular values of common annihilator. The peaks in the SOD signal correspond to the different groups of pulses present in the signal. 52

5.3 Fetal QRS reconstruction of signal from Set A of Physionet Challenge 2013 54

5.4 Fetal R peak detection of signal from Set A of Physionet Challenge 2013 with annotation 55

5.5 Fetal R peak detection of signal from Set B of Physionet Challenge 2013 without annotation 56

5.6 Fetal R peak detection of signal from Set B of Physionet Challenge 2013 without annotation 57

5.7 Algorithm for detecting P and T waves 58

5.8 P and T wave detection on 3 lead ECG signals 61

5.9 Top: Reshaped A_5 coefficients, (a)-(c):P and T wave detection on ECG signal with simulated baseline wander and EMG noise at SNR 0dB, (d)-(e): Detected P and T wave instances juxtaposed onto the original, clean ECG signal 63

List of Tables

4.1 Comparison of mean and standard deviation of estimated K with various levels of noise across 100 simulations 41

Chapter 1

Introduction

Electrocardiography (ECG) has been used by clinicians for decades to diagnose cardiac abnormalities in patients. Although the clinical need has remain unchanged, the methodologies and applications have expanded due to the improvements in sensing and signal processing. It remains the easiest, cheapest and most convenient method to diagnose cardiac diseases in patients which is the reason for its widespread use up till today.

The ECG is captured by using surface electrodes, on a patient's skin, which measure the electrical activity in the heart which in turn is generated through electrical nodes and muscular contractions and relaxations. Therefore, any rhythm irregularities caused by abnormal nodal or muscular changes will be reflected. Specific placement of these electrodes can be used to detect Myocardial Infarctions (MI), or heart attacks, expanding ECG's use espe-

cially in emergency medicine.

As mentioned in the previous paragraph, placement of the electrodes is critical as protocols have been developed using specific patterns of placement for clinical diagnosis. Single leads are mainly used in consumer devices for heart rate calculation or other simple metrics which do not require much additional information. To clinically monitor a patient for a longer term, one day to one week, three or more leads are used so as to compensate for artifacts or signal corruption in any channel. In the clinical setting, twelve leads are used for thorough monitoring. This is not currently practical for home monitoring as it is uncomfortable and disruptive.

In clinical practice, ECG machines incorporate some automated diagnostic algorithms such as heart rate and simple arrhythmia detection. This field has been explored extensively and several methods have been used and tested for commonly occurring arrhythmias. However, there is a shift in the way medicine is being practised. Data collection is no longer strictly within the confines of a hospital but a continuous process which captures every second of the day. The understanding that arrhythmias occur at any time of the day and during various activities is the driving force behind small wearable technologies which can seamlessly integrate into everyday life. As the descendants of the Holter monitor, these small devices are made possible by the quantum advances in micro and nano sensors, in advanced communication

and storage systems and in new, innovative compression methods.

Along with continuous monitoring comes the challenges of data storage and transmission amongst other things. The advances in compression have been developed to address these concerns. Compression reduces the amount of information transmitted and significantly reduces the amount of data that needs to be stored. This can be achieved with one of several compression techniques such as compressive sensing, FRI, spline based methods and wavelet methods. Some methods such as FRI, spline and wavelet methods need to be tailored to the type of signal it acts upon, whereas compressive sensing can be applied to a large range of signals.

Since FRI deals with a specific class of signals, non-bandlimited signals in particular, there was a need to develop a generalised model. The basis of the FRI method begins with defining a Dirac by its location and amplitude parameters. A sampling and reconstruction scheme based on the Fourier coefficients was then developed around the parameterized model. By adding width and asymmetry parameters, VPW-FRI has expanded the traditional FRI to model signals as a sum of pulses which can cover a large range of signals.

The VPW-FRI algorithm treats the ECG signal as a sum of pulses. Each cardiac cycle, on average, requires seven pulses to model it accurately. This differs from traditional sampling schemes in that the compression ratio of

VPW-FRI is event dependent meaning that fewer samples are needed at lower heart rates and more samples at higher heart rates when there are more events occurring.

In this thesis, only signal compression, reconstruction and an automated diagnosis, based on the VPW-FRI sparse model, will be discussed. The clinical significance of the findings will be discussed generally. However, doctor's annotations or specific comments on the clinical relevance will not be included.

There are two advantages to heart rate based sampling. One is that, for the majority of people, a large part of the day is spent at rest and only a fraction of the day is spent at elevated heart rates.This means that only a few pulses per minute need to be used during the rest periods. Secondly, with an event driven sampling technique, specific events can be identified from compressed samples. Wave and event detection can be done from identifying the pulses directly rather than employing a string of other algorithms.

An alternative view of healthcare data and how it is processed will be presented here. The VPW-FRI algorithm provides an integrated solution for compression, detection and de-noising. The nature of the algorithm allows it to be flexible in its capabilities. In Chapter 4, the order estimation of VPW-FRI, or the optimal estimation of the number of pulses required, will help to address an earlier problem with FRI where the number of pulses

had to be known *a priori*. As will also be shown in the subsequent chapters, various waves within the ECG will be detected using both single and multichannel signals. In Chapter 5, specific applications like fetal HR monitoring will be presented as they are directly related to events occurring in the ECG signal. Fetal heart rate monitoring is an important application as it shows the flexibility of VPW-FRI in detecting waveforms. The work performed in this thesis allows the VPW-FRI signal to be broken down into subspaces which correspond to specific features. Therefore, features of the fetal waveform could be identified by reconstructing the specific subspace. This could be applied to any scenario involving removing noisy pulses and source separation using single or multiple channels. This could be extended to multimodal environments where common features across various signals could be extracted to identify which channels contribute specifically to the detection of particular features.

Subsequent work also show hybrid models which allow FRI to be combined with wavelets to achieve desired results. The use of this hybrid model also demonstrates the use of different kernels to suit specific applications.

The thesis will be organized as follows. Chapter 2 will provide a study on ECG and FRI as well as VPW-FRI. The novel work which expanded VPW-FRI to cover multichannel ECG signals will be detailed in Chapter 3. Order estimation for ECG heart beats developed in this thesis will be explained in

Chapter 4 and the various methods of ECG wave detection will be presented in Chapter 5. The thesis will be concluded in Chapter 6.

Chapter 2

Background

2.1 Electrocardiography

The ECG describes the electrical activity of the heart recorded by electrodes on the body surface. The voltage variations measured by the electrodes are caused by action potentials of the excitable cardiac cells as the cardiac tissue contracts. The resulting heartbeat in the ECG is manifested by a series of waves whose morphology and timing convey information which is used for diagnosing diseases that are reflected by disturbances of the heart's electrical activity.

The heart is essentially a muscle which contracts to pump blood to the lungs and the rest of the body. The heart consists of four chambers, the left and right ventricle and the left and right atrium. The de-oxygenated

blood from the body enters the right atrium where it is passed through a valve to the right ventricle where it is then pumped to the lungs to be re-oxygenated. The oxygenated blood returns to the heart into the left atrium where it passes through a valve to the left ventricle where it is pumped to the rest of the body through the aorta.

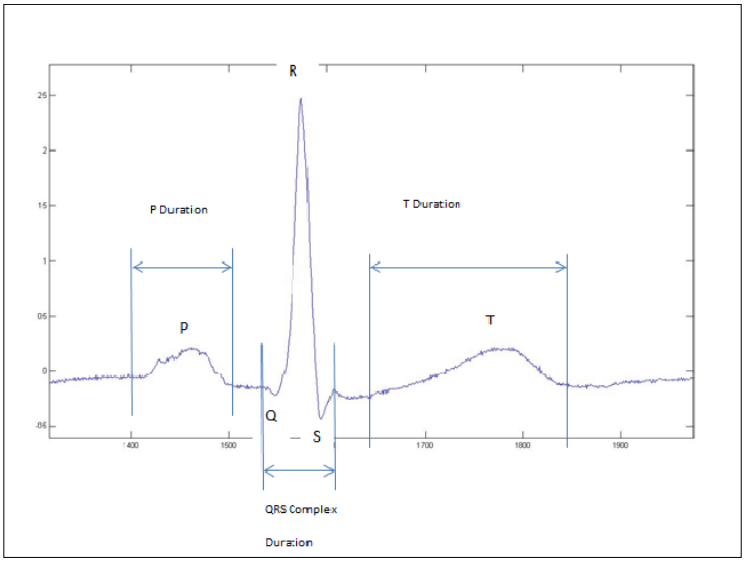

Figure 2.1: ECG waveform and its constituent waves

Figure 2.1 represents an example of an ECG waveform which represents the electrical activity of the heart. The P wave reflects the depolarization of the left and right atria. The atrial repolarization cannot be seen as it is masked by the much larger QRS complex. The duration is usually less than 120ms. The QRS complex reflects the depolarization of the right and left ventricles which would normally last 70-110ms. The morphology of the

QRS complex is highly variable. It is the largest amplitude waveform in the ECG of around 2-3mV. The T wave represents ventricular repolarization and extends about 300ms after the QRS complex. The position of the T wave depends on the heart rate, becoming narrower and closer to the QRS at rapid heart rates. The RR interval represents the length of a ventricular cycle [4].

There are different methods for acquiring ECG. The number of leads usually ranges from one to twelve with the number of leads depending on the application. Single lead ECG machines are usually found on sports and fitness devices whose primary goal is to determine heart rate. This means the ECG can be taken from any part of the body as the form of the wave does not have an impact on heart rate calculation. For Holter monitors or 3 lead ambulatory ECGs, the patient wears a monitor for a short period which can last for up to a couple of days. The goal is rhythm monitoring so three leads are sufficient for clinicians. Rhythm is consistent across leads so the multiple leads are to combat noise. In a stress test, a twelve lead ECG is recorded whilst the patient is subjected to various physical stress levels either on a treadmill or a bicycle. Twelve leads are used because arrhythmias appear in different leads where the electrical vectors in the heart radiate in different directions. The lead placement can be seen in Fig. 2.2.

From a wave detection standpoint, the R wave is the easiest to detect and is often the easiest way to calculate heart rate which is the inverse of the RR

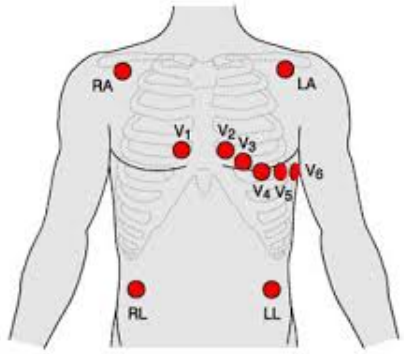

Figure 2.2: Lead placement for ECG. Three lead ECG uses leads LA, RA, LL and RL whereas the twelve lead ECG uses all the leads including V1-6.

period. The morphology of the waves is an important factor in the reading of an ECG in addition to the location of the P, QRS and T waves. The waves occur without delay across all the leads which means the waves may occur at the same time but their morphology may differ. One example would be when waves are inverted across certain channels and it may be indicative of certain types of arrhythmias.

2.2 Finite Rate of Innovation

The famed Shannon theorem on sampling is considered one of the most fundamental works in sampling theory. It provided a framework for analogue to digital signals and is the basis of almost all data processing. Shannon's work on bandlimited signals is limited when dealing with signals outside this

bandlimited subspace.

Sparsity has become a trend in the age of big data. Modeling a signal on its sparsity rather than its bandlimitedness has its advantages. Sparsity allows for greater compression and faster transmission. It also requires more creative models which allow the signal to be expressed in new ways and new features to be observed.

The FRI method described by *Vetterli et al.* [1, 8] is one such method. It begins with a sparse signal defined by

$$x(t) = \sum_{k=1}^{K} \sum_{k' \in Z} b_k \delta(t - t_k - k'\tau), \tag{2.1}$$

where $x(t)$ is a $\tau-$periodic stream of K Diracs with amplitude b_k and location $t_k \in [0, \tau]$. The signal can also be expressed by its Fourier coefficients as shown in Eq. (2.2),

$$x(t) = \sum_{m \in Z} \underbrace{\frac{1}{\tau} \sum_{k=1}^{K} b_k \underbrace{e^{-j2\pi m t_k/\tau}}_{u_k^m}}_{X[m]} e^{j2\pi m t/\tau} \tag{2.2}$$

where $X[m]$, $m = -M, \ldots, M$ represents the Fourier coefficients. The signal $x(t)$ has $2K$ degrees of freedom per period, the b_k amplitudes and t_k locations, which implies that the rate of innovation[1] is $\rho = \frac{2K}{\tau}$. The signal $x(t)$ is convolved with a sinc kernel with bandlimit $B \geq \rho$ represented by Eq. (2.3),

$$\phi(t) = \sum_{k' \in Z} sinc(B(t - k'\tau)) = \frac{sin(\pi B t)}{B\tau sin(\pi t/\tau)}. \tag{2.3}$$

[1]Rate of innovation = degrees of freedom per unit of time

The convolved signal, $y(t) = x(t) * \phi(t)$, is sampled uniformly at $t = nT$ and results in Eq. (2.4)

$$\begin{aligned} y[n] &= \langle x(t), sinc(Bt - n) \rangle \\ &= \frac{\tau}{N} \sum_{|m| \leq \lfloor B\tau/2 \rfloor} X[m] e^{j2\pi mn/N}, \end{aligned} \tag{2.4}$$

where $n = 1 \ldots N$ and $N \geq B\tau$.

This completes the model for the acquired stream of Diracs through a sinc sampling kernel. The problem now shifts to recovering the parameters b_k and t_k from the spectral values $X[m]$, since those values represent knowledge of the entire stream of Diracs.

One method of solving this involves the *Prony method* which the authors in [1] have labelled the *annihilating filter* method , seen in Eq. (2.5), which assists in solving $\mathbf{XA} = \mathbf{0}$ where $\mathbf{X}$ is a Toeplitz matrix constructed of the spectral values $X[m], m = -K, ..., K$.

$$\begin{bmatrix} X[0] & \ldots & X[-K+1] \\ X[1] & \ldots & X[-K+2] \\ \vdots & \ddots & \vdots \\ X[K-1] & \ldots & X[0] \end{bmatrix} \cdot \begin{bmatrix} A[1] \\ A[2] \\ \vdots \\ A[K] \end{bmatrix} = 0, \tag{2.5}$$

where $A[k]$, $k = 1 \ldots K$, represent the annihilating filter coefficients. Practically, Eq. (2.5) can be solved using a Singular Value Decomposition (SVD)

or null space algorithms. Consider the Z transform of the annihilating filter represented by Eq. (2.6),

$$A(z) = \sum_{k=0}^{K} A[k] z^{-k} = \prod_{k=0}^{K-1} (1 - u_k z^{-1}), \tag{2.6}$$

where $u_k = e^{\frac{-j2\pi m t_k}{\tau}}$. The location parameter, t_k, can be returned by taking the zeros of $A(z)$. The amplitudes, b_k, can then be found by solving a Vandermonde system of equations formed using the u_k values,

$$\begin{bmatrix} 1 & 1 & 1 & 1 \\ u_0 & u_1 & \dots & u_{K-1} \\ \vdots & \vdots & \dots & \vdots \\ u_0^{K-1} & u_1^{K-1} & \dots & u_{K-1}^{K-1} \end{bmatrix} \cdot \begin{bmatrix} b_0 \\ b_1 \\ \vdots \\ b_{K-1} \end{bmatrix} = \begin{bmatrix} X[0] \\ X[1] \\ \vdots \\ X[K-1] \end{bmatrix}. \tag{2.7}$$

Equation (2.7) has a solution when the values of u_k are unique, $u_k \neq u_l, \forall k \neq l, k, l = 0, \dots, K-1$.

Since the parameters b_k and t_k completely describe the signal, the signal can be reconstructed to machine precision.

2.3 VPW-FRI

Variable Pulse Width FRI extends the traditional FRI model by introducing two more parameters, namely, width and asymmetry [2, 3]. This allows

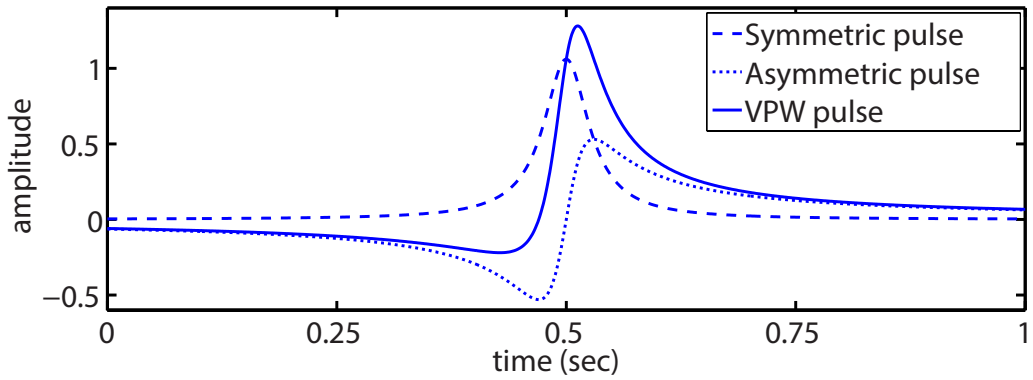

Figure 2.3: Symmetric and asymmetric components of a VPW-FRI pulse

the original Dirac model to be generalised into a pulse model with variable widths and asymmetry. Pulses with fixed widths have been dealt with before in ultrasound imaging [14] but this is the first work to fit a sum of variable width pulses to model waveforms.

The VPW-FRI pulse, as can be seen in Fig. 2.3, can be represented by

$$X[m] = X_1[m] + X_2[m], \tag{2.8}$$

where

$$X_1[m] = \sum_{k=0}^{K-1} c_k e^{-2\pi(a_k|m|+jt_k[m])/\tau} \tag{2.9}$$

and

$$X_2[m] = -\sum_{k=0}^{K-1} d_k sgn(m) e^{-2\pi(a_k|m|+jt_k[m])/\tau}. \tag{2.10}$$

The variable $X_2[m]$, as seen in Eq. (2.10), is the Hilbert transform of $X_1[m]$ and both their spectra are symmetric. The Cauchy Lorentz distri-

bution is described by Eq. (2.9), with an amplitude c_k, and the asymmetric component represented by Eq. (2.10), with an amplitude d_k. Modifying the roots from a Dirac to a Cauchy Lorentz distribution allows the model to have variable width, which is represented by the a_k parameter in Eqs. (2.9) and (2.10).

The sampling of signals and solving for these parameters is very similar to the steps in Section 2.2. Sampling occurs at a minimal rate of innovation $2K$ where K is the number of estimated pulses. Similar to FRI, the number of pulses must be known *a priori*. A solution, defined as the order estimation of VPW-FRI, which is the optimal estimation of the number of pulses required for the accurate reconstruction of the signal through an oversampling scheme will be presented in Chapter 4. The Annihilating filter in Eq. (2.5) is used to solve for the locations, t_k, from the Toeplitz matrix of Fourier samples. To ensure a stable solution, only the roots of the annihilating filter which occur inside the unit circle are admitted and the rest are disposed of. The roots are then arranged in a Vandermonde, similar to Eq. (2.7), and the complex amplitudes are obtained. The c_k and d_k parameters are the real and imaginary components respectively.

The continuous time signal, $x(t) = \sum_{k=0}^{K-1} x_k(t)$, which represents K continuous time VPW-FRI pulses, can be recovered by applying the inverse Fourier transform of $X[m]$. The continuous time representation of the k^{th}

pulse is

$$\begin{aligned} x_k(t) &= \sum_{n\in\mathbb{Z}} c_k \frac{a_k}{\pi(a_k^2 + (t - t_k - n\tau)^2)} \\ &+ \sum_{n\in\mathbb{Z}} d_k \frac{t - t_k - n\pi}{\pi(a_k^2 + (t - t_k - n\tau)^2)} \quad . \end{aligned} \tag{2.11}$$

An alternate formula for $x_k(t)$ that avoids the infinite sum is given by:

$$x_k(t) = \frac{c_k}{\tau}\frac{1 - |z_t|^2}{(1 - z_t)(1 - z_t^*)} + \frac{d_k}{\tau}\frac{2\mathrm{Im}\{z_t\}}{(1 - z_t)(1 - z_t^*)} \tag{2.12}$$

where $z_t = e^{2\pi(-a_k + i(t - t_k))/\tau}$.

2.4 Sparse sampling in ECG

The field of sparse sampling in ECG mainly focused on compression of the signals. This section will focus on the parametric approach rather than those of compressed sensing and wavelets. One of the key techniques with this approach is that of FRI which models the signal and uses derived parameters for reconstruction. Hence the signal is fully described by these parameters.

2.4.1 FRI in ECG: ECG as splines

The first attempt in parameterizing ECG was done by *Hao et al.* [6] who modelled the QRS as non-uniform linear splines. The motivation stated in that paper was to preserve the QRS complex as non uniform linear splines

and the remainder of the ECG signal as a $4-9\ Hz$ lowpassed signal. This approach was able to introduce heart rate (HR) dependent compression techniques. Each heartbeat would require $2K$ parameters, where K is the number of splines, for the QRS and $8-18$ samples for the Nyquist sampled residue ECG signal.

They used a modification of the original FRI [1] as the non uniform spline of degree R required an extra step. The signal was modelled as

$$x(t) = x_{BL}(t) + x_{NUS}(t) \tag{2.13}$$

with a continuous time Fourier series coefficients where L is the bandwidth of the residue signal. The $2K$ contiguous Fourier samples for the non uniform spline are taken outside of the bandwidth L as seen in Eq. (2.14)

$$X_{NUS}[m] = X[m], m \in [L+1, L+2K]. \tag{2.14}$$

Since the non uniform spline is of degree $R = 1$, the signal is differentiated $R + 1 = 2$ times to obtain Diracs, as seen in Eq. (2.15)

$$X_{NUS}^{(R+1)}[m] = (i2\pi m/\tau)^{R+1} X_{NUS}[m], m \in [L+1, L+2K]. \tag{2.15}$$

The locations and weights of the Diracs are found as per Section 2.2. The reconstructed spline can be found by integrating $R + 1 = 3$ times from the Diracs.

The compression ratio (CR) is defined as $2K + L$ and a CR value of between 14.0 to 19.1 was reported for various values of L and K.

In general, this scheme was found to be unstable as the number of splines had to be very accurate which otherwise lead to incorrect reconstruction. This was corroborated by *Baechler et al.* [3].

2.4.2 VPW-FRI in ECG: ECG as pulses

Subsequent work with FRI in ECG was conducted by [2, 3]. They used the VPW-FRI model in Section. 2.3 to sample and reconstruct the ECG signal. The main aim of the work was to maximise the CR and reconstruction accuracy with an additional focus on processing of noisy signals.

The application of VPW-FRI was first proposed by *Quick et. al* [2]. It described the use of FRI and the theoretical basis behind the de-noising of the signal. Two methods for denoising were described. Firstly, the method of De Moor was described as the optimal method of solving the least squares optimization problem described by [8]. However, it proved to be slow in its execution. However the authors found that the Cadzow method described by [8] proved to provide satisfactory performance whilst speeding up performance, though it was sub-optimal. However, the best performance was still provided by the ESPRIT algorithm which will be described in detail in

Chapter 3.

The ideal number of VPW-FRI pulses needed to accurate modeling and reconstruction for a single heart beat was found to be seven, $K = 7$. This was derived experimentally. A method involving oversampling to estimate the optimal number of pulses, K, required for a segment of ECG, known as the order estimation, will be presented in Chapter 4. The achievement in [2] was to show that only 14 complex, or 28 real numbers, were needed to model a heartbeat. These seven pulses were sufficient to cover all the different morphologies of an ECG heart beat. Any additional pulse would simply contribute to the reconstruction of noisy elements in the signal. Therefore it was vital that optimal order estimation would be part of any future work on the subject. This will be discussed in Chapter 4.

In [3], the reconstruction was dealt with in further detail. A method was developed to segment each heart beat based on the locations of the detected QRS compelxes [15]. The VPW-FRI algorithm would then be applied to each individual ECG heart beat.

Also, the matter of stability of the reconstruction was addressed. The roots of the annihilating filter need to be located within the unit circle for stability. One of the considerations was to force all the roots inside the unit circle through magnitude correction. The other was to simply discard all the roots outside the unit circle. The method of projecting the roots back into

the unit circle at a fixed distance was found to be optimal.

Finally, a comparison was done between VPW-FRI, the Amplitude Zone Time Epoch Coding (AZTEC) [25] and Compressive Sensing (CS) [26]. The Signal to Residue Ratio (SRR) was used as the metric for reconstruction accuracy. It is defined by

$$SRR = 20\log_{10}(\frac{||x||_2}{||x-\hat{x}||_2}), \tag{2.16}$$

where $\hat{x}$ is the reconstructed version of the original signal x.

It was found that VPW-FRI outperformed AZTEC in terms of modeling accuracy. Using the MIT-BIH Arrhythmia Database [28], for a CR of 10, AZTEC had an SRR of 22 dB as compared to an SRR or 25.4 dB for VPW-FRI. To achieve a similar performance to VPW-FRI, AZTEC could only manage a CR of 8.

2.5 Data

This section describes the data used in performing the ECG analysis. The data comes from two sources which have different collection methods and were collected for different purposes.

2.5.1 TTSH Data Set

The data used was 12 lead Stress ECG data recordings from Tan Tock Seng Hospital, Singapore. The subjects were patients who were undergoing treadmill ECG tests as recommended by their physician. All subjects voluntarily signed an agreement to have their anonymised data used for research purposes. The tests conducted were under the conditions of the BRUCE protocol [27] which is a stress ECG protocol where the incline and speed of the treadmill are increased at intervals of 3mins. The data was collected using the GE Marquette CASE Stress System with the T2100 treadmill. This data, collected from 6 patients, varied in length from 12 minutes to 20 minutes long depending on the patients fitness level, cardiac health and the discretion of the physician. The leads recorded are I, II, III, aVR, aVL, aVF, V1, V2, V3, V4, V5 and V6. A simple and concise write up about the leads and their significance can be found in [27]. The data is sampled at 200Hz.

2.5.2 NTU Data Set

A second set of data was obtained using the CleveMed BioCaptureTMwhich can record up to eight channels simultaneously. A sampling rate of 960Hz with a resolution of 12 bits/sample was used to capture the data. A three lead ECG, leads I, II and III, were captured using wet electrodes. The

subjects were made to perform various tasks which included raising of arms, picking up objects from the ground, brushing teeth, jogging, push ups and climbing stairs. A total of twenty sets of data were collected from three volunteers. These tests were designed to observe the artefacts generated on an ambulatory ECG device during the daily routine of regular people. Artefact free segments as well as segments with EMG and motion artefact were chosen to test robustness.

Chapter 3

Multichannel ECG Analysis using the Common Annihilator

Multichannel signals exist in many field including communications such as MIMO antenna arrays as well as biomedical signals which use multiple channels to confirm diagnoses or offer different points of view.

In [4], *Hormati et al.* describe a multichannel system where the events in each channel share a common location across all the channels. This allows robustness in reconstruction of multichannel FRI signals. This method was adapted to VPW-FRI in [9] where the common support principle was extended to the pulse model.

The common annihilator has applications in compression and in feature detection which will be used for QRS detection in Section 5.2. The common

annihilator also has de-noising built into it using the FRI ESPRIT de-noising algorithm [7].

In this chapter, compression of multichannel ECG signals using the common annihilator will be presented. Results will be shown to compare the accuracy and efficiency of the reconstruction between the single and multichannel methods.

3.1 Common Annihilator Method

It would make sense to simplify the calculation of the locations of the pulses in a multichannel signal with common support. Not only does it save computational complexity but it also adds further compression. In ECG, the common annihilator is especially applicable, as the rhythmic cardiac events occur at the same time regardless of where they are measured.

In FRI, the roots of the common annihilator are where the u_k values are calculated, as seen in Section 2.2. This can be used to directly derive the t_k values for the signal. This is usually solved by feeding the Toeplitz matrix into an SVD. By changing the inputs to the SVD, this could be modified for use in the multichannel scenario.

The common annihilator can be described as

$$\begin{bmatrix} \mathbf{X_1} \\ \mathbf{X_2} \\ \vdots \\ \mathbf{X_M} \end{bmatrix} \cdot \begin{bmatrix} A[1] \\ A[2] \\ \vdots \\ A[K] \end{bmatrix} = 0. \tag{3.1}$$

where $\mathbf{X_m}$ represents the Toeplitz matrix of the m^{th} channel and $\{A[k]\}_{k=1}^{K}$ represents the annihilating filter coefficients similar seen in Section 2.2. The elements and construction of $\mathbf{X_m}$ can be described as

$$X_m = \begin{bmatrix} X_m[0] & \dots & X_m[-K+1] \\ X_m[1] & \dots & X_m[-K+2] \\ \vdots & \ddots & \vdots \\ X_m[K-1] & \dots & X_m[0] \end{bmatrix}. \tag{3.2}$$

The roots of the resulting common annihilator, u_k, can be used to derive the t_k locations which would be common across all the channels.

The ESPRIT method for de-noising FRI signals [7] will be used in this case as well. It is essentially a subspace method that utilizes singular vectors from the SVD. The SVD can be described as,

$$\mathbf{X} = \mathbf{USV^H} \tag{3.3}$$

where $\mathbf{U}$ is a $((M \times (2K+1)) \times (2K+1))$ unitary matrix, $\mathbf{S}$ is a diagonal matrix containing the singular values, $\mathbf{V}$ is also a unitary matrix of size $(2K+1) \times (2K+1)$and $\mathbf{V^H}$ is the Hermitian conjugate matrix.

The matrix $\mathbf{V}$ is then used to estimate the de-noised signal,

$$\overline{\mathbf{V}} = \underline{\mathbf{V}} \cdot \Phi_H, \tag{3.4}$$

where $\overline{(\cdot)}$ and $\underline{(\cdot)}$ denote the operation of omitting the first and last row of $(\cdot)$, respectively. The conjugates of the eigenvalues of Φ_H will yield the roots of the annihilating filter and not the filter coefficients as seen in Eq. (2.5). For a detailed proof, please refer to [7].

3.2 Results

The data used in this chapter was the TTSH Data Set from Section 2.5. One hundred data segments, each 2 seconds long, were used to test the efficiency and accuracy of compression and reconstruction. The measure used for reconstruction accuracy is the SRR described in Eq. (2.16). As can be seen in Fig. 3.1, all twelve channels were reconstructed accurately without much trouble. Figure 3.4 shows the mean SRR and its standard deviation across all the channels. This was compared to the scenario where each of the 12 channels were sampled and reconstructed individually. Predictably, reconstructing each individual channel would be more accurate and consistent than using the common annihilator. However, the margin is under $3dB$ and is visually imperceptible. Also, the low standard deviation shows consistency in reconstruction across the channels.

This is weighed by the fact that the common annihilator provides greater compression as seen in Fig. 3.2. At a HR of $60bpm$, the CR goes up from 7.1 to 8.5. Since, VPW-FRI is HR dependent, at very high HR, the CR would naturally go down.

The denoising capabilities can be seen by Fig. 3.3. The algorithm worked well as it maintained the features of the signal and the signal was not distorted despite the noise of AWGN at $10dB$.The denoising capabilities extend to more intense levels of noise, however more sophisticated automated order estimation is needed as the correct subspace needs to be identified.

In [3], a comparison was performed with single channel VPW-FRI and AZTEC compression [25] and it was shown that for a fixed compression rate, VPW-FRI outperformed AZTEC by 8dB which still is worse than the 3dB reduction in the SRR from multichannel VPW-FRI to single channel VPW-FRI.

3.3 Discussion

The common annihilator was a reliable reconstruction method for multichannel signals with common support. Although it resulted in a slight drop in accuracy, it made up for it in the additional CR it provided.

The VPW-FRI algorithm models the ECG signal well, and hence it is able

to extract the true signal from the noise. This allows it to extract features despite distortions and this would aid in data from ambulatory devices which suffer from high levels of noise.

The R peak detection is robust and workable as it is based soundly in the VPW-FRI theory. This means it works in scenarios with heavy noise. The robustness of the algorithm is balanced by the fact that it would be computationally more expensive than other algorithms due to the SVD.

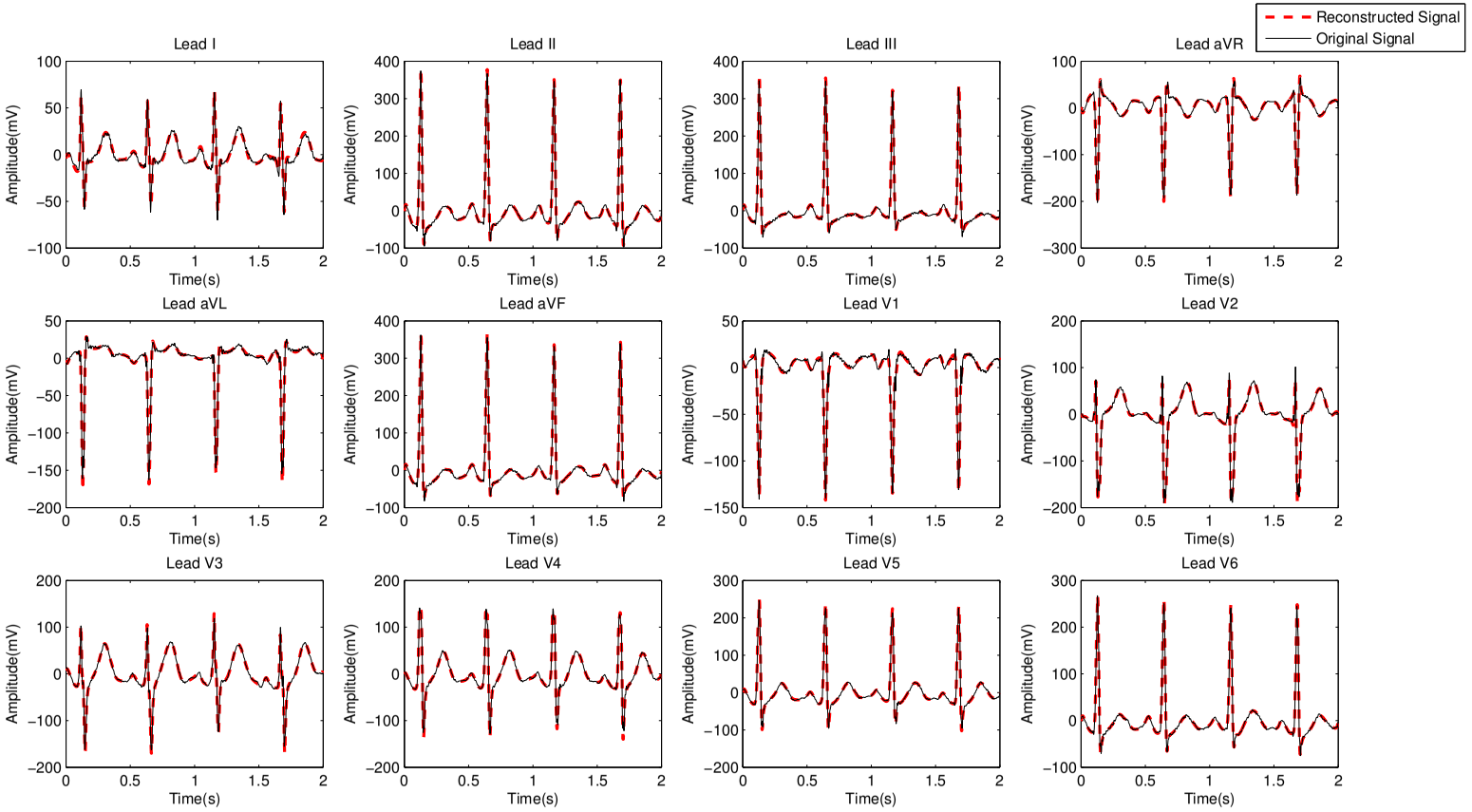

Figure 3.1: Reconstruction of 12 lead ECG from Data Set A.

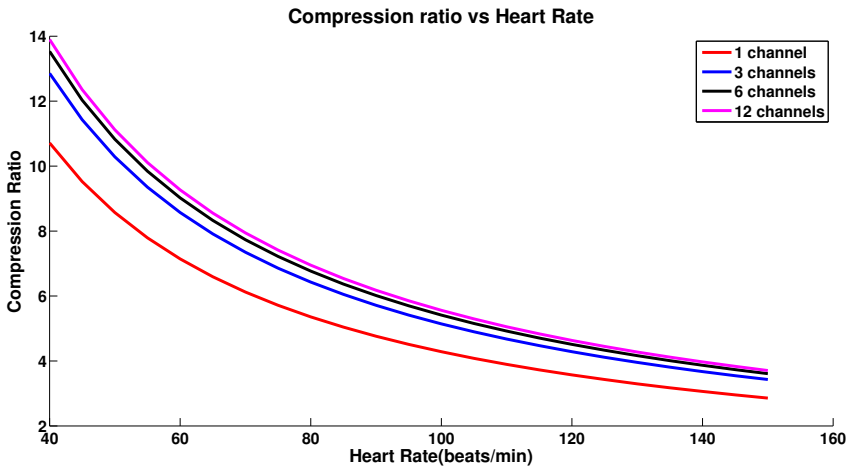

Figure 3.2: Compression ratio of VPW-FRI vs Heart Rate

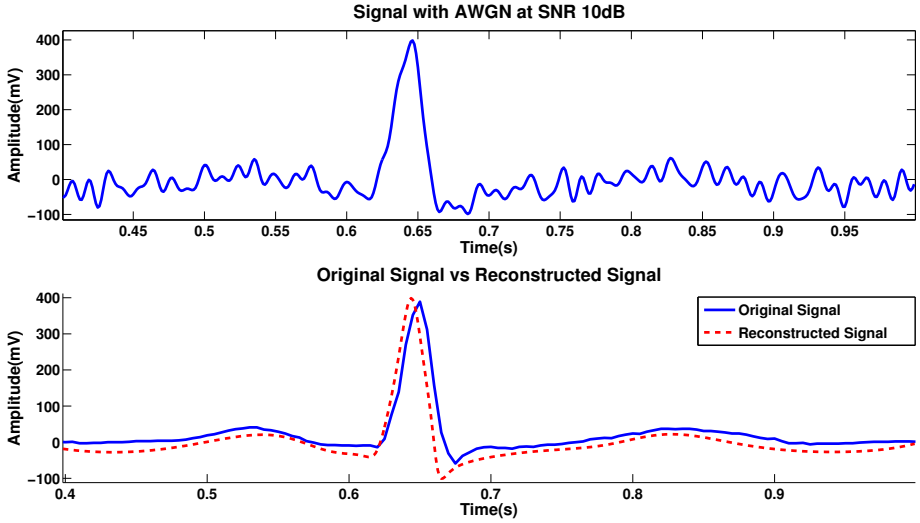

Figure 3.3: De-noising of an ECG heart beat with added AWGN $10dB$.

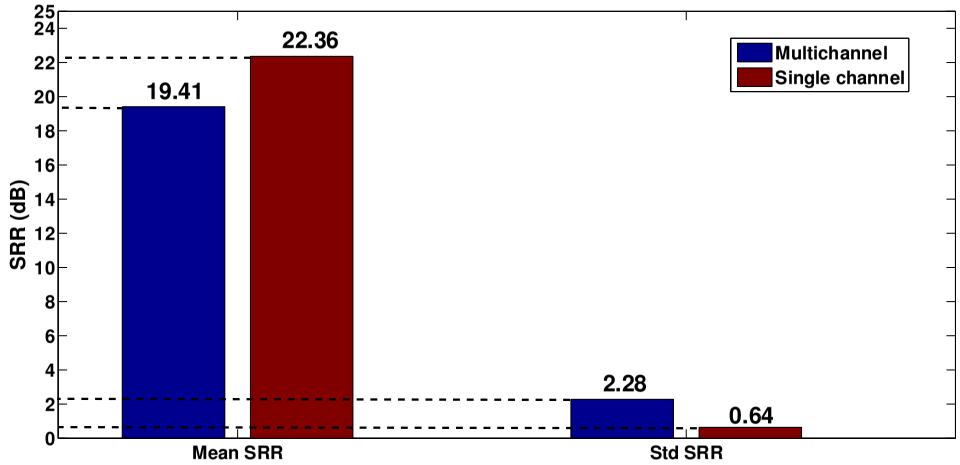

Figure 3.4: Comparison of modeling accuracy using single lead and multichannel ECG

Chapter 4

Order Estimation of VPW-FRI pulses applied to ECG

4.1 Background

Order estimation for Electrocardiogram (ECG) signals in VPW-FRI previously involved manually estimating the number of pulses, K, either for single or multiple heart beats. This was done by multiplying the number of beats by a fixed number pulses per beat. The optimal number of pulses per beat was empirically found to be seven [2].

However, it has been found that a close approximation of the order of each segment of data can be found automatically by further analysing the properties of the singular values.

In this chapter, a method for estimating the order of ECG heart beats will be presented. The number of pulses required for accurate reconstruction of an ECG heart beat will be estimated using the Second Order Differential (SOD) method. Order estimation is important as it affects the CR. Also, the number of features in the heart beat can be identified for use in feature detection.

The two methods will be tested on the TTSH and NTU Data Sets from which segments with single heart beats will be extracted.

4.2 Second Order Differential Method

The method presented in this section utilizes the second order difference(SOD) to determine the order as well as other distinguishable features. In MATLAB, a rough first order difference can be achieved using the `diff()` command. The positive peaks in the second order difference correspond to the points where there is a positive change in gradient. The location of the last peak above a threshold would correspond to the estimate of the order. This threshold can be defined as

$$\alpha = \begin{cases} 2\sigma & \text{if } 0 \leq K \leq K_1 \\ \\ \frac{\sigma}{75} & \text{if } K_1 \leq K \end{cases} \tag{4.1}$$

where α is the threshold, σ is the standard deviation of the second order difference and t_1 is the index after the first peak as can be seen in Figure 4.1.

The K value refers to the variable in the equation

$$X[m] = \sum_{k=0}^{K-1} c_k e^{-2\pi(a_k|m|+jt_k[m])/\tau} - \sum_{k=0}^{K-1} d_k sgn(m) e^{-2\pi(a_k|m|+jt_k[m])/\tau}, \quad (4.2)$$

or the number of pulses used to reconstruct a signal. The points detected

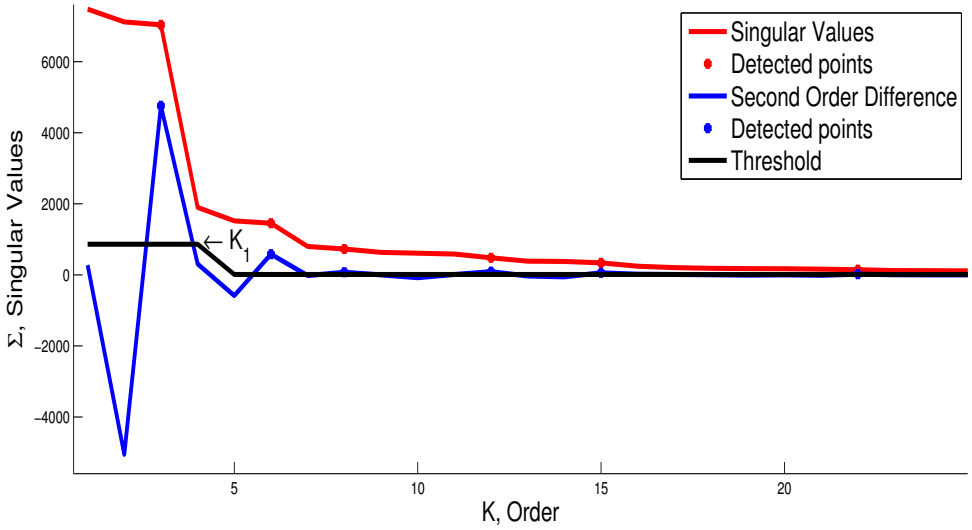

Figure 4.1: Singular Values vs Second Order Difference

on the SOD reflect groups of points which are similarly scaled. These are features on the ECG signal such as QRS complexes, P and T waves. The QRS complexes can be easily detected, which will be explained further in Section 5.2 but the P and T waves are less obvious and require further investigation. To deal more effectively with noise, the number of pulses for the entire segment is limited to 12 times the number of detected QRS complexes. Any detected points beyond that limit would not be considered for reconstruction as they are deemed to be extraneous information.

4.3 Results

Segments of data containing only a single beat will be used in this section. Signals with and without noise will be analysed and the results of the order estimation for both methods will be compared. The data used in this section

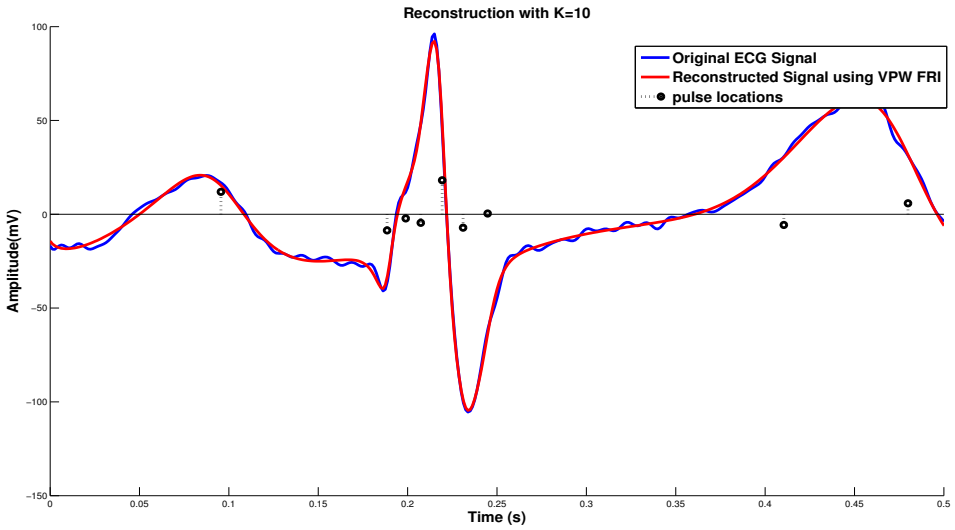

Figure 4.2: Reconstruction of Lead 2 using $K = 10$

would come from the TTSH data set unless otherwise stated. As can be seen in Figure 4.2, when the signal is relatively noise free, the reconstruction is of a very high quality. The order can be estimated easily and clearly by the second order difference method. Figure 4.3 shows the singular values and the results of the method presented in Section 4.2. In the case of Figure 4.2, the second order difference method estimated $K = 10$. This was repeated over 50 beats from the same recording and the average K estimated was 9.85 for

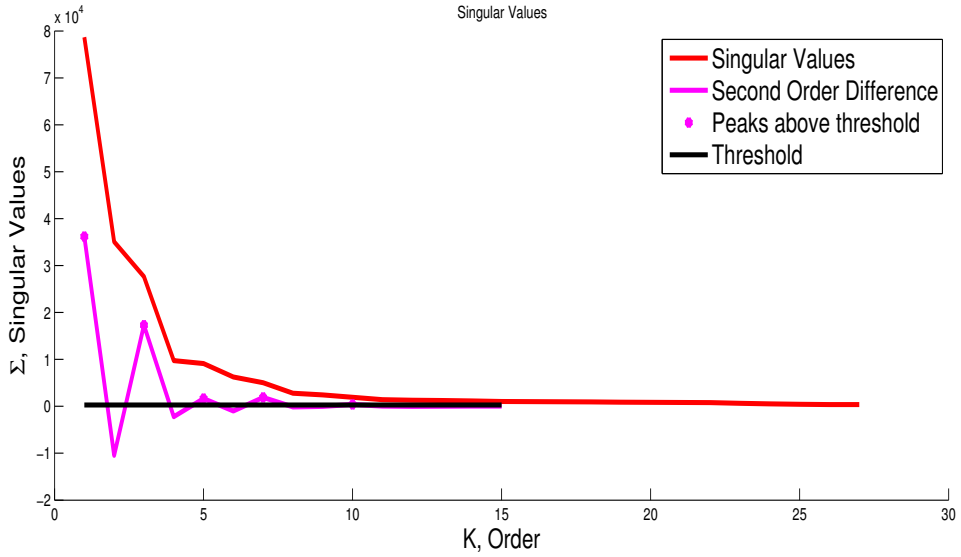

Figure 4.3: Singular values with Order Estimation

the second order difference. Figure 4.4 shows the mean SRR of all the leads

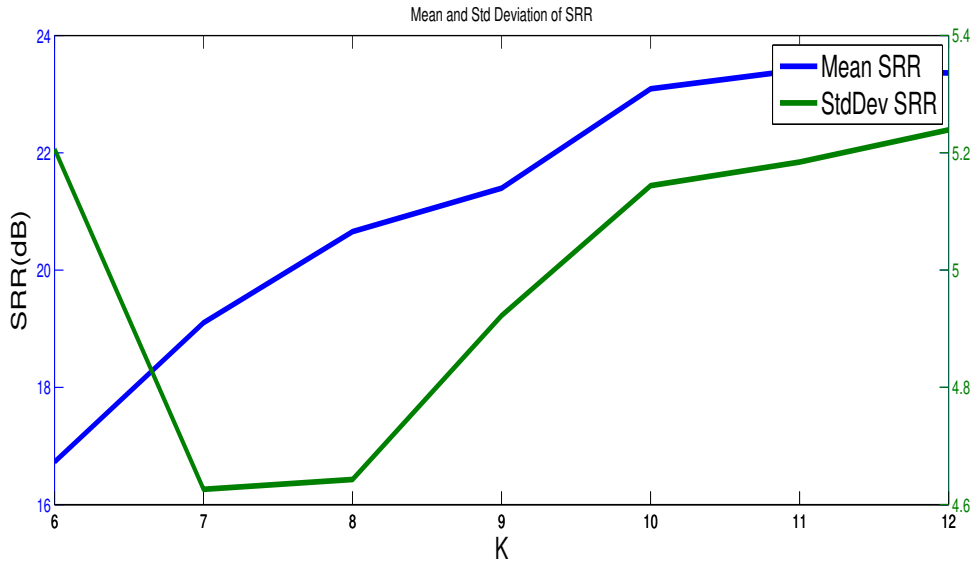

Figure 4.4: Mean and standard deviation of SRR for different values of K

reconstructed for various orders of K. The plot shows both an overestimate and underestimate of K and compares it with the estimate provided by the two methods. It shows the SRR does not improve significantly after $K = 10$. Before $K = 10$, the SRR improves significantly especially from $K = 8$ to $K = 10$. An estimate of $K = 7$ might seem enough but upon visual inspection, $K = 9$ and 10 provide a more defined Q wave. Clinically, this has some significance as a common sign of cardiac abnormality would be the QT interval.

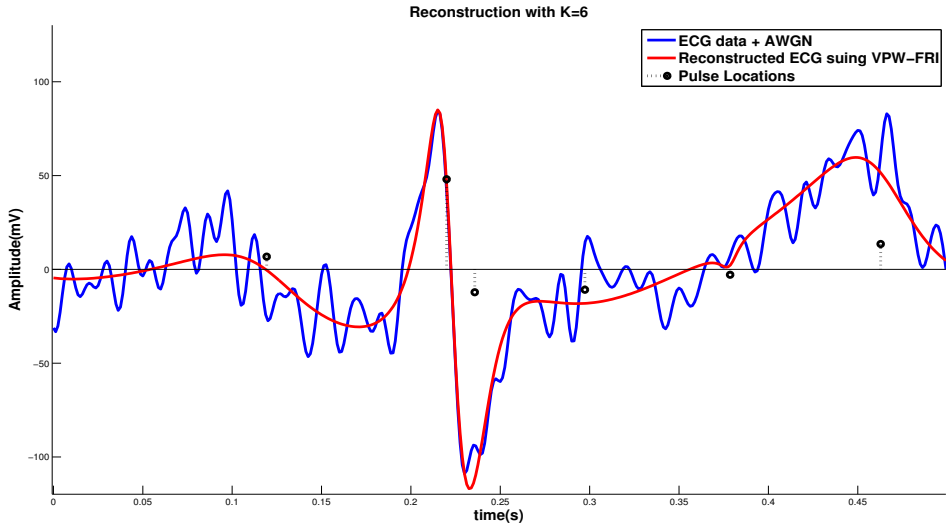

Figure 4.5: Reconstruction of Lead 2 with AWGN at 10dB

For the noisy case, Additive Gaussian White Noise (AWGN) was added to all the channels to simulate muscle noise or other high frequency artefacts. Baseline wander was not considered in this section as it can only be better

Noise SNR(dB)	Order Estimate, K, using Second Order Difference	
	mean	std
0	11.2600	1.6613
5	8.9800	3.0911
10	7.3000	2.5406
15	6.6700	1.7469

Table 4.1: Comparison of mean and standard deviation of estimated K with various levels of noise across 100 simulations

visualised in longer segments. In Figure 4.5, the same segment in Figure 4.2 is used with 10dB of AWGN. The reconstruction is performed using the estimated order of $K = 7$ which was provided by the SOD method.

The estimated order in the case of noisy signals varies according to the level and intensity of the noise. At lower SNRs, there may be peaks towards the tail end of the second order difference, caused by the noise, which could cause the estimated K to be large. This can be clearly seen in Table 4.1 where at the lower SNRs, large values of K are estimated whereas at the higher SNR values, the estimated K is much lower. However, at lower levels

of noise (SNR$\geq$ 15), the results are consistent. The lower estimate of K is expected as a lower level of detail is detected and reconstructed as can be seen when comparing Figures 4.2 and 4.5. As can be seen in Figure 4.6, the peaks on the second order difference for the clean segment are more prominent especially below $K = 10$. However, for the noisy signal, there are a few detected peaks after $K = 10$ which would correspond to spurious peaks caused by the noise. One possible way of eliminating this would be to only consider a maximum of 10 pulses per beat which would then mean the noisy segment would have an estimate of $K = 3$ which would involve the QRS complex and the T wave. That would be a good estimate to determine the number of features which would be accurately reconstructed from the noisy data.

The peaks correspond to the various features shared by all the leads. The pulses with the highest energies would correspond to the initial peaks. The first 2 peaks correspond to the QRS complex. The third peak does not always form the QRS and on many occasions forms the T wave instead especially in segments with large T waves. This was especially true in data set B where there are only 3 leads and the third peak would consistently reconstruct the T wave.

Figure 4.7 shows the second lead from an ECG segment from the Data Set B presented in Section 2.5. The noise in the signal is inherent and is most

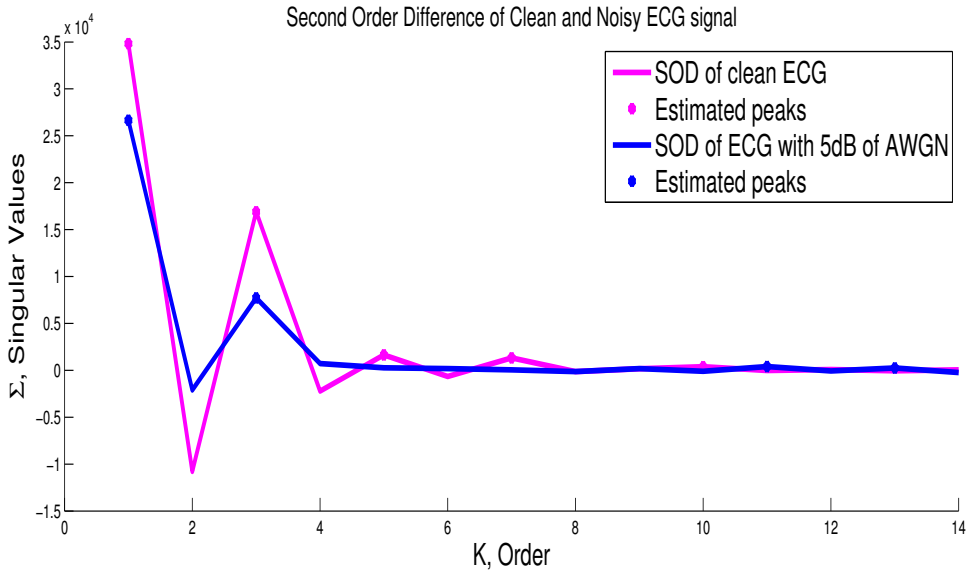

Figure 4.6: Comparison of second order difference of clean ECG signal and the same segment with 5dB of AWGN

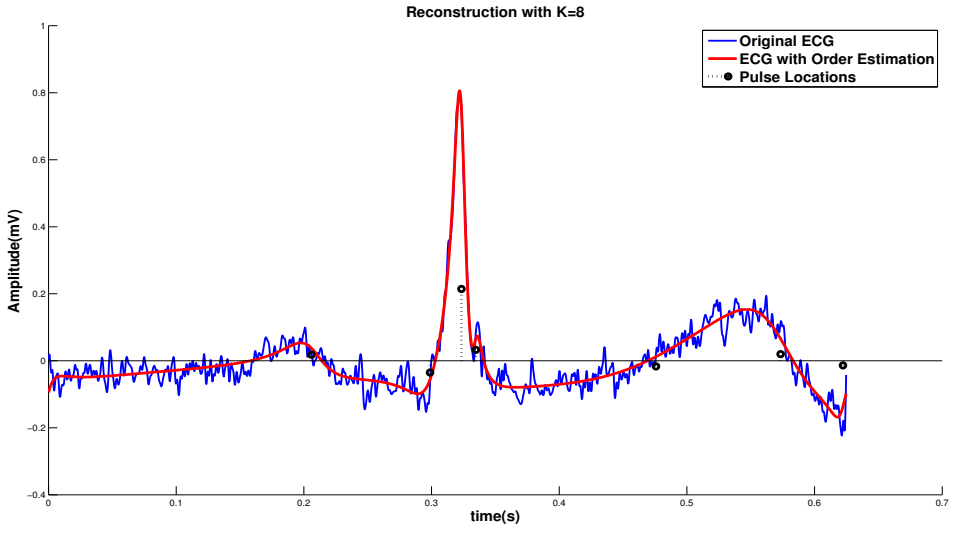

Figure 4.7: Reconstruction of noisy ECG with $K = 8$

likely to be muscle noise. Both methods again estimated $K = 8$. However, the Q wave is not clearly seen and this is expected as it may be masked by noise and may only become clearer if more pulses are used.

The solution presented in this section is very specific to FRI and therefore few other comparisons exist. The overestimation of pulses, or oversampling, was introduced by [8], but the method presented in this section is non-iterative.

4.4 Conclusion and Future Work

There is still work to be done primarily in artefact removal. Identifying the pulses associated with the baseline wander would allow for a model based artefact removal scheme. This could be implemented by modifying the width constraint to include pulses below a certain width but this has not yielded consistent results yet.

Another thing that could be looked into would be P and T wave detection using the order estimation. For an adult ECG, only QRS complexes can be accurately determined using the subspace but there is a possibility of using order estimation to detect other waves.

Chapter 5

Wave Detection in ECG

5.1 Background

Wave detection is vital in automated ECG diagnosis as it is the key through which clinicians are able to more efficiently identify segments in which cardiac conditions are present. In Holter monitors and other clinical equipment, only the strips containing arrhythmias detected by the software are printed as it is very inefficient and time consuming for clinicians to analyse 72 hours of data manually.

In this Chapter, various methods of wave detection in ECG will be presented using FRI. The three main features in an ECG signal, the P, T and QRS waves, will be detected using an assortment of FRI methods. Also fetal R peak detection, a special case of the R peak detection, will be presented.

5.2 R Peak Detection

The detection of the R peak in an ECG signal is one of the most basic diagnostic tools available. It is the most prominent feature and it is used to calculate heart rate (HR) and the R-R interval. Many methods include using the energy signal, wavelets and real time filters [15].

5.2.1 Method

The method presented here is based on the common annihilator in Chapter 3 described by

$$X = USV^H, \tag{5.1}$$

where the diagonal of S represents the singular values, is also applicable on single channel signals. The trick here would be to identify the correct subspace corresponding to the R peak pulses. Given that it uses a subspace approach, it is very robust even in the presence of noise as only the pulses associated with the R peak are retrieved.

The R peaks would have the greatest energy or singularity out of all the waveforms in an ECG. This corresponds well to the VPW-FRI model. The roots of the common annihilator, or annihilating filter, closest to the unit circle would represent the R peaks. These roots are represented by the highest singular values from the diagonal of the matrix **S** in Eq. (5.1). The

group of pulses with similar characteristics can be identified using the ratio, E_n, of consecutive elements of the diagonal of $\mathbf{S}$.

$$E_n = S_n/S_{n+1}, \qquad n = 1, \ldots, N-1 \tag{5.2}$$

where S_n represents the n^{th} element of the diagonal of $\mathbf{S}$. The group of pulses representing the R peaks can be found by locating the value of n corresponding to

$$\max_{n \in 1,\ldots,N-1} (E_n). \tag{5.3}$$

The first $K = n$ pulses would correspond to the R peaks. This can be achieved by reconstructing the first $K = n$ pulses using Eq. (2.5) to (2.7). The inverse of the difference between adjacent t_k values would yield the instantaneous heart rate.

5.2.2 Results

The data from the TTSH Data Set was used in this section. The same 100 segments of data used in Section 3.2. The R peak detection proved to be robust and resistant to noise. The proposed algorithm in Section 5.2.1, only missed 3 beats in the 100 segments used for testing with $0db$ AWGN. At $5dB$ AWGN , the algorithm detected all the R peaks. This proved the success of the subspace approach taken to identify waves. The R peak detection is robust and workable as it is based soundly in the VPW-FRI theory. This

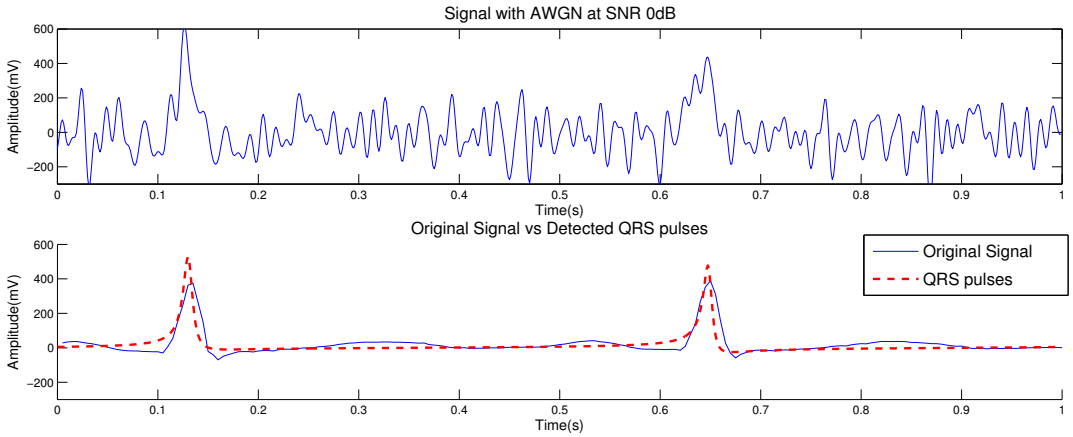

Figure 5.1: R peak detection on an ECG signal with AWGN $0dB$

means it works in scenarios with heavy noise. The robustness of the algorithm is balanced by the fact that it would be computationally more expensive than other algorithms due to the SVD.

This is usually a trivial problem, but the reason it is discussed in this thesis is that it is model based and can be calculated with minimal additional computation.

5.3 Fetal R Peak Detection

Fetal HR monitoring is an important tool to check the foetus' health. Any variation in the HR would be cause for concern an increase in the HR could indicate distress. Many methods of fetal HR monitoring are used. Doppler devices are used, along with ultrasounds, invasive and abdominal ECG. Of

these methods, the abdominal ECG is the most cost effective and easiest to perform. The invasive method involves placing electrodes on the foetus' scalp and is not convenient. The downside to the abdominal ECG is that the fetal ECG power is very low compared to that of the mother's, so it may not be apparent in the abdominal ECG.

The work in [24], on which this section is based upon, was inspired by the Physionet Challenge 2013, which challenged entrants to devise robust fetal R peak detection methods.

A comprehensive data set was released for the Challenge which was split into sets A, B and which composed of four channels. Set A was the training set with the R peaks being annotated for reference. Set B was the test set without annotations and Set C was the hidden set for evaluation of the contestants. In this section, only samples in Data Set A and 100 samples in Data Set B were used which were each $60s$ long and were sampled at $360Hz$.

The VPW-FRI method for extracting pulses will be used in this section. Other methods which were used in the competition included maternal ECG removal [10, 12], matched filtering [10, 11] and PCA [10, 12].

5.3.1 Method

This application helped to test the ability of VPW-FRI to distinguish between pulses of different characteristics. This was briefly discussed in Section 5.2 where the R peaks were extracted from the signal. This work will extend that and and prove VPW-FRI can perform source separation in single or multichannel environments. The common annihilator method in Chapter 3 will be used.

For analysis, the data will be split into one second segments. The baseline wander has to be removed for optimal results so a $1Hz$ high pass filter is performed on each segment.

For $\Sigma = diag(S)$, where S is the singular matrix in $X = USV^H$, the discrimination of the groups of pulses would be similar to that in Chapter 4. The second order difference (SOD), $\frac{d^2\Sigma_k}{dk^2}$, will be used to identify the groups of pulses with similar characteristics. The singular values, Σ, can be defined as

$$\Sigma_k = \sqrt{|c_k^2 + d_k^2|}, \tag{5.4}$$

where c_k and d_k are the amplitudes of the symmetric and asymmetric components respectively. This is an extension from [7] which dealt with traditional FRI signals only. The c_k and d_k components are constrained by the equation

$$X[m] = \sum_{k=0}^{K-1} c_k e^{-2\pi(a_k|m|+jt_k[m])/\tau} - \sum_{k=0}^{K-1} d_k sgn(m) e^{-2\pi(a_k|m|+jt_k[m])/\tau}, \quad (5.5)$$

which is the Cauchy -Lorentz distribution and the Hilbert Transform of the Cauchy Lorentz. This would mean that the amplitudes are inversely proportional to the width of the pulse hence, the largest Σ values would belong to the narrowest pulses. The wider, large amplitude pulses therefore tend to be a sum of multiple pulses. This corresponds well to the assumption of the first group of pulses belonging to R peaks. The fetal R peaks are also sharp, however they are of a smaller amplitude than those of the mother. Therefore, they can be found from the second and third peaks in the SOD as shown in Fig. 5.2.

The algorithm to detect the fetal R peaks is as follows:

1. Identify the order of the signal, K_N, using the SOD method in Chapter 4. Identify the number of maternal R peaks, K_R, using the same SOD method.

2. Reconstruct the signal excluding the maternal R peaks, from K_{R+1} to K_N^{th} pulse, where K_1 to K_R pulses correspond to the maternal R peaks

3. Sample the resultant signal from Step 2 again and decompose using VPW-FRI

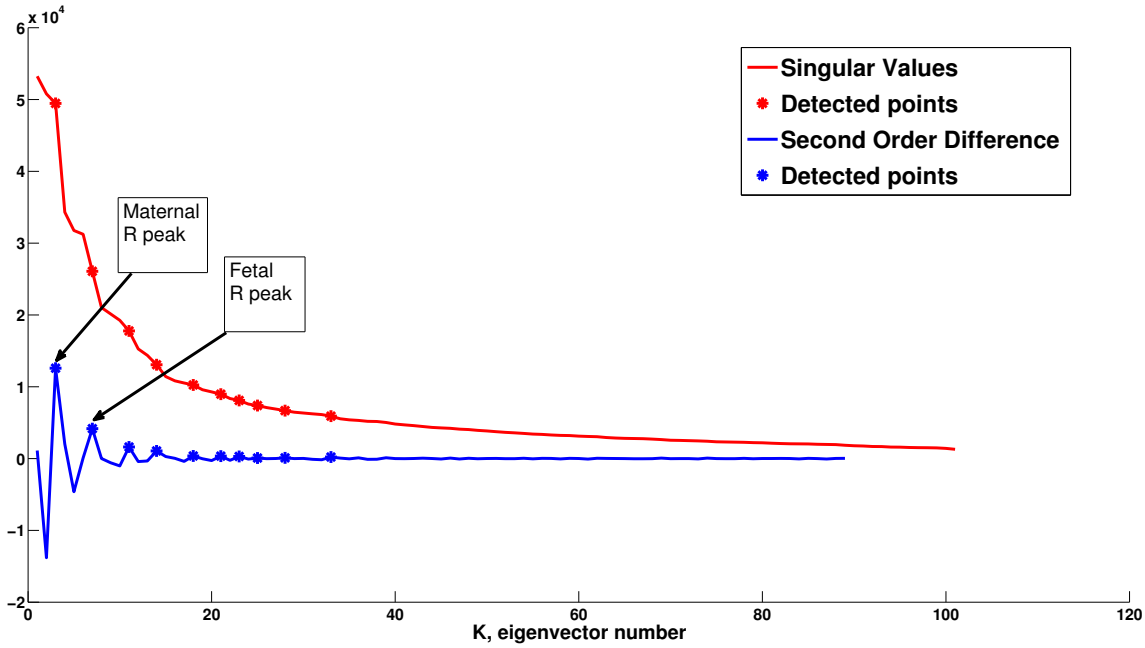

Figure 5.2: Singular values of common annihilator. The peaks in the SOD signal correspond to the different groups of pulses present in the signal.

4. Reconstruct the parameters for the first and second group of pulses using the SOD method. A visual example of identifying the groups of pulses can be seen in Fig. 5.2.

5. Only reconstruct pulses with a width $a_k < 0.1 * \tau$, where τ is the period of the segment. This is intended to specifically select the fetal R peak pulses which have small widths as compared to other forms of noise.

The above algorithm can be executed using one or more channels. This incorporates many elements of what other contestants used like the maternal

R peak filtering, and has the advantage of executing them all within the framework of VPW-FRI.

5.3.2 Results

The results varied between the data sets. With annotations present in Data Set A, the accuracy of the method presented in the previous section could be verified. In set A, out of 25 data sets, the algorithm performed well in 19 sets. In the other 6 sets, the algorithms was not able to pick out the fetal R peaks accurately. Figures 5.3 and 5.4 are some examples of data from set A. Figure 5.3 shows the estimation of the R peak location against the annotation. This was one of the data sets which worked well. Even at $1.8s$ where the fetal R peak was part of the maternal QRS, the algorithm was able to identify it. In Fig. 5.4, the reconstruction of the fetal R peak is shown. Again, at $0.2s$, the algorithm was able to reconstruct the fetal QRS complexes despite one of them beign embedded in the maternal QRS. The detection rate for the 19 sets was 98.2% with an accuracy of $\pm 7ms$ whereas the detection rate for the remaining 6 sets was 41%. This was attributed to the fact that the fetal R peaks were too small and embedded in intense noise which made them undetectable. A more intensive sorting process would have led to overfitting of the data.

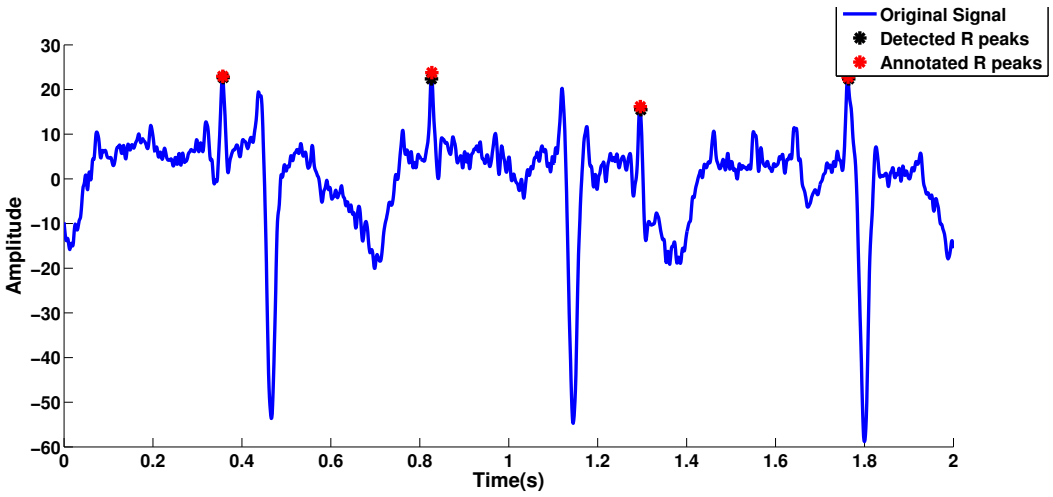

Figure 5.3: Fetal QRS reconstruction of signal from Set A of Physionet Challenge 2013

Since Set B was not annotated, only visual inspection of the results could be done. In Figs. 5.5 and 5.6, the fetal R peaks were identified despite the baseline wander and the EMG noise.

From the visual inspection, the results seem to be of roughly the same accuracy as that of Set A. Comparing the winners of the Challenge to our results would not make sense given that they were judged on a hidden set of data. However, just as a mention, the winner had a detection rate of 96%.

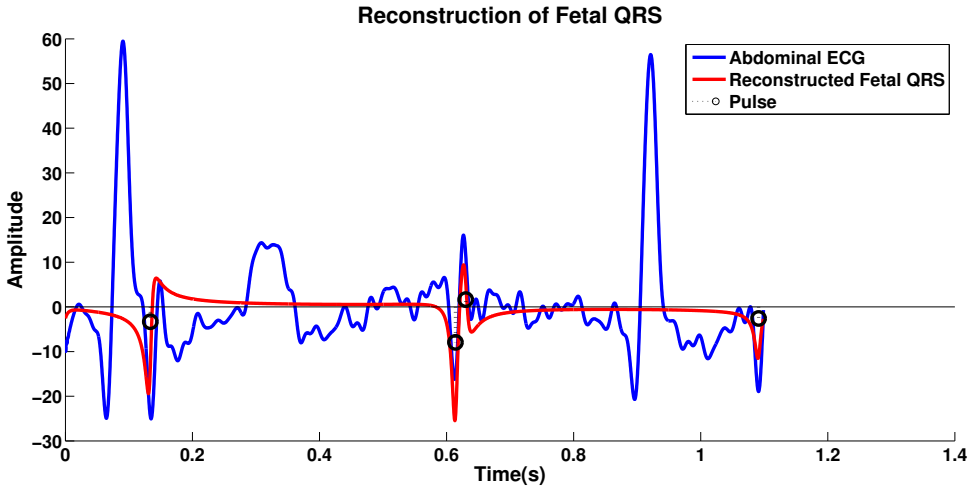

Figure 5.4: Fetal R peak detection of signal from Set A of Physionet Challenge 2013 with annotation

5.4 P and T Wave Detection with Gaussian Kernel

The P and T waves represent valuable information regarding the atrial and ventricular activity of the heart. By identifying the locations, the waves can be further studied and their morphologies can be analysed. Furthermore, in the presence of noise, the signals become obscured easily and low amplitudes waves are easily distorted.

Various methods have been used for detection of P and T waves, namely the First and Second Derivative [16] slope [22], ICA [19] and energy signature [21]. The method presented in this section [23] however, analyses all

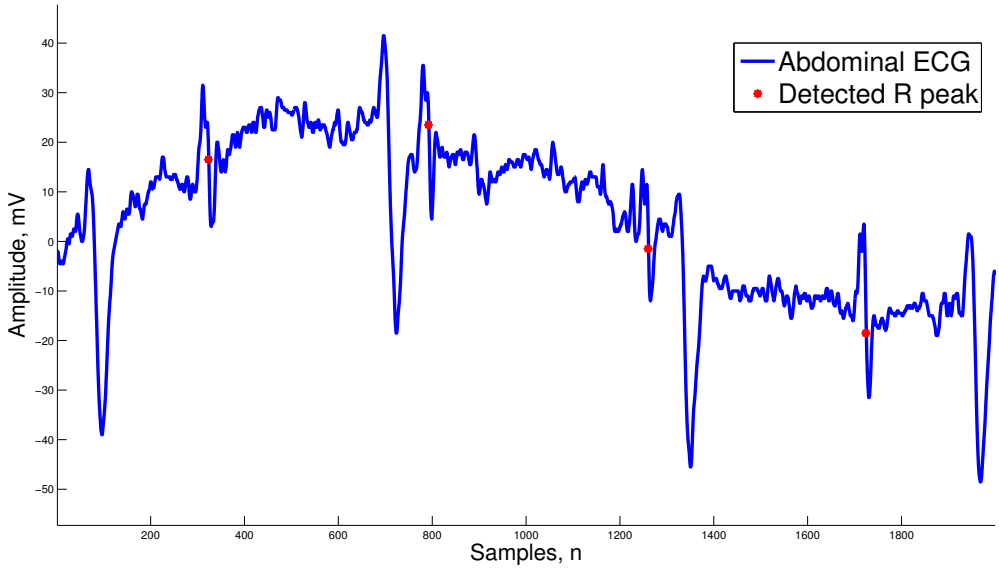

Figure 5.5: Fetal R peak detection of signal from Set B of Physionet Challenge 2013 without annotation

the channels at once by compressing them into one signal using a 2D wavelet transform. This would have benefits for noisy or low amplitude signals as will be seen later in the section.

5.4.1 Method

As seen in Fig. 5.7, the first step is to identify the QRS locations in order to identify the appropriate windows. This is achieved using the method in Section. 5.2. These QRS locations are then mapped onto the approximation

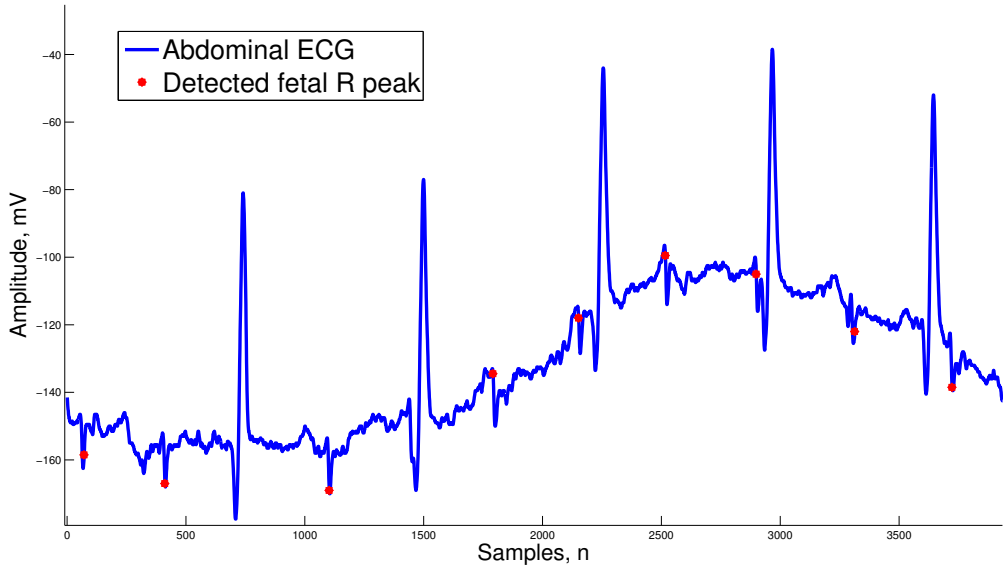

Figure 5.6: Fetal R peak detection of signal from Set B of Physionet Challenge 2013 without annotation

coefficients $\hat{t}_{QRS}$, using a scaling factor h, followed by a shift g,

$$\hat{t}_{QRS} = (h \times t_{QRS}) + g. \tag{5.6}$$

The hat notation is used to represent the values mapped onto the approximation coefficients, A. The raw data, $x[m, n]$, where m is the number of channels and n is the sample index, is processed first using a 2D wavelet transform. A Biorthogonal 5.5 wavelet is used [20] which was found to be appropriate for ECG signals. The signal $x[m, n]$ is decomposed into the respective approximate, vertical, horizontal and diagonal coefficients which are represented by A, V, H, D respectively. In this section, only the A coeffi-

cients will be used. Since the bandwidth required is under $30Hz$, the signal was decomposed to the third level. The approximate coefficients A, which would be in matrix form are reshaped into a row vector.

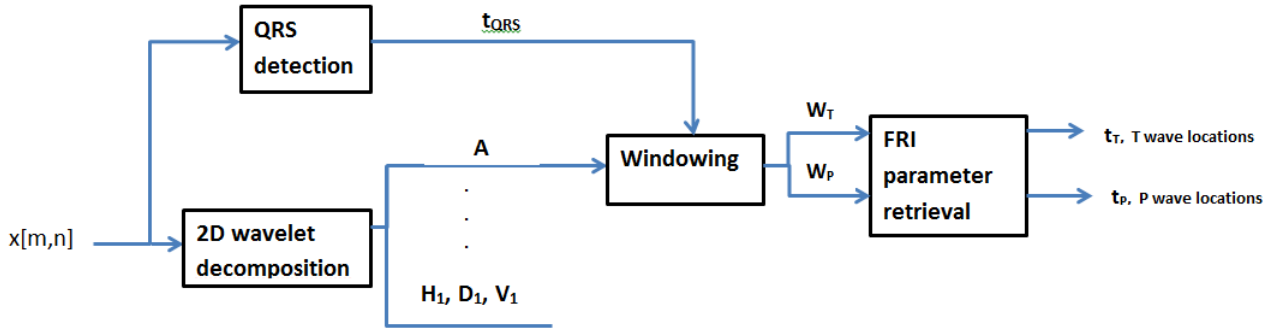

Figure 5.7: Algorithm for detecting P and T waves

As seen in Fig. 5.7, the first step is to identify the QRS locations in order to identify the appropriate windows. This is achieved using the method in Section. 5.2.

The windows for both the P and T waves are then calculated. Physiological limits [18] of the durations of the QRS, P and T wave are used to determine the windows. The constants $w = 0.1$sec, $v = 0.08$sec, $u = 0.2$sec, $z = 0.4$sec, $s = 0.1$sec are used to denote the QRS, ST, PR, QT and P wave duration respectively [18]. The windows are defined by

$$\tau_P = [\hat{t}_{QRS} - 0.5\hat{w} - \hat{u}, \hat{t}_{QRS} - 0.5\hat{w} - \hat{u} + \hat{s}] \tag{5.7}$$

$$\tau_T = [\hat{t}_{QRS} + 0.5\hat{w} + \hat{v}, \hat{t}_{QRS} - 0.5\hat{w} + \hat{z}], \tag{5.8}$$

where τ_P and τ_T represent the windows for the P and T waves respectively. The constants w, v, u, z, s are based on an assumption of sixty beats per minute and hence would have to be weighted by a factor of $\frac{60}{HR}$ depending on the R-R interval calculated.

Next, a Gaussian kernel would be used for the FRI sampling and reconstruction. The number of events would be assumed to be $K = 1$ and hence, only 2 uniform samples would be needed per window. The samples, y_n are given by

$$\begin{aligned} y_n &= \sum_{k=0}^{K-1} c_k e^{-(t_k - nT)^2/2\sigma^2} \\ &= \sum_{k=0}^{K-1} (c_k e^{-t_k^2/2\sigma^2}) e^{nt_k T/\sigma^2} e^{-n^2T^2/2\sigma^2}, \end{aligned} \tag{5.9}$$

where σ represents the standard deviation of the Gaussian kernel and $n = 0, ..., N-1$. The σ value is known *a priori*.

If we let $S[n] = e^{-n^2T^2/2\sigma^2} y_n$, $a_k = c_k e^{-t_k^2/2\sigma^2}$, $u_k = e^{nt_k T/\sigma^2}$, then Equation (5.9) is equivalent to

$$S[n] = \sum_{k=0}^{K} a_k u_k^n, \qquad n = 0, \ldots, N-1. \tag{5.10}$$

Equation (5.10) can be solved using the annihilating filter method and the u_k values can be retrieved. The t_k values are then given by

$$t_k = \frac{\sigma^2 \ln u_k}{T}, \tag{5.11}$$

where $t_{k,P}$ and $t_{k,T}$ represent the locations in the τ_P, and τ_T, windows respectively. The amplitudes are then given by

$$c_k = a_k e^{t_k^2/2\sigma^2}. \tag{5.12}$$

The locations of the P and T waves in the approximation coefficients,A, can be represented by

$$\hat{t_P} = \hat{t}_{QRS} - 0.5\hat{w} - \hat{u} + t_{k,P} \tag{5.13}$$

and

$$\hat{t_T} = \hat{t}_{QRS} + 0.5\hat{w} + \hat{v} + t_{k,T}, \tag{5.14}$$

where $t_{k,P}$ and $t_{k,T}$ represent the location of the peak in the τ_P and τ_T windows respectively.In order to calculate the locations in the time domain, the reverse of the shifts and scaling in Eq. (5.6) can be performed.

5.4.2 Results

The data used would be TTSH Data Set from Section 2.5. The length of segments of data used for testing is 4096 samples. Artifacts such as AWGN and baseline wander were added to test the robustness of the algorithm.

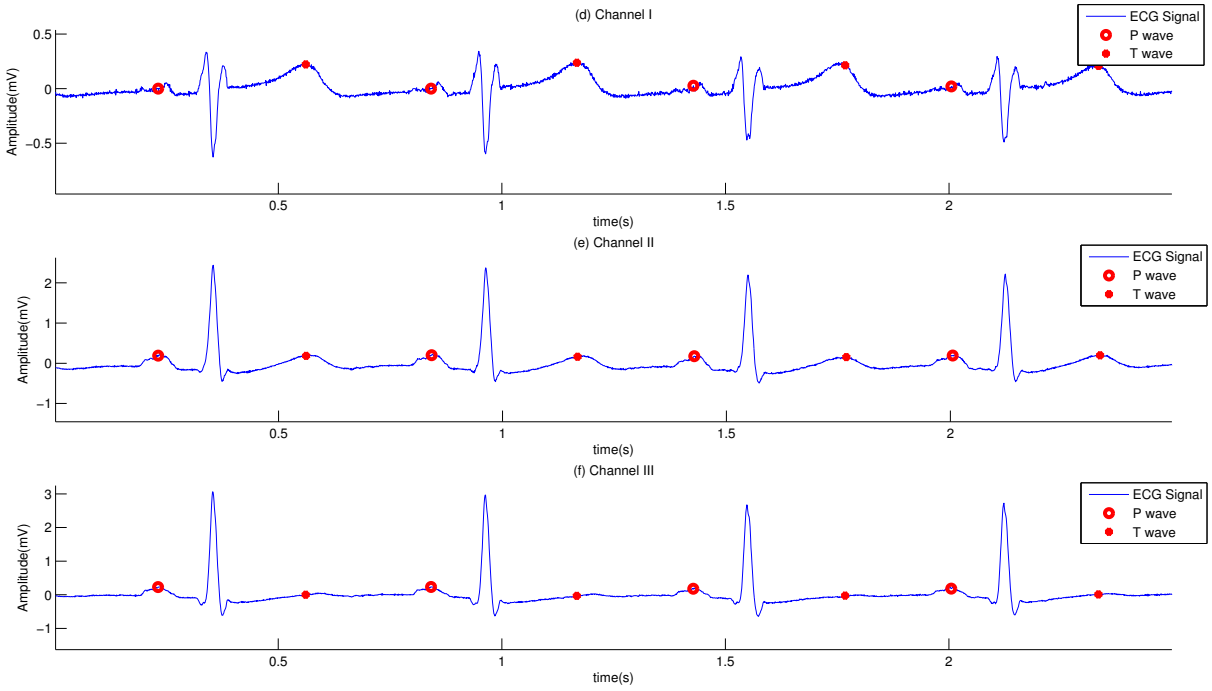

Figure 5.8: P and T wave detection on 3 lead ECG signals

Figure 5.8 shows the ability of the algorithm presented in this section to detect P and T waves in a normal scenario. The P and T waves were detected accurately which validates the use of the 2D wavelet transform to decompose the multichannel signal.

In Fig. 5.9, the noisy case is presented. The signal was distorted with AWGN $0dB$ and baseline wander was added using a $4th$ order polynomial. In Fig. 5.9(a)-(c), the detection of the P and T waves on the noisy signals are shown. In Fig. 5.9(d)-(f), the same detected P and T waves were juxtaposed onto the original clean signal to show the accuracy of detection. In cases of

noise at $0dB$ or above, the detection is accurate. However, below $0dB$, the performance degrades significantly.

In this section, the gold standard would be a clinician's annotation. However, due to the time consuming nature of the work, the annotations could not be obtained and the results were based on visual inspection.

5.5 Discussion

The VPW-FRI algorithm has proved to be verstaile enough to handle different types of feature detection. In Section 5.4, VPW-FRI could have been used as well to detect the P and T waves, but it was done using the traditional FRI with Gaussian kernel to demonstrate the variety of methods possible under the FRI umbrella.

The feature detection almost serves as a source separation method and the list of features that could be detected could be of great use to clinicians in automated diagnosis and remote monitoring.

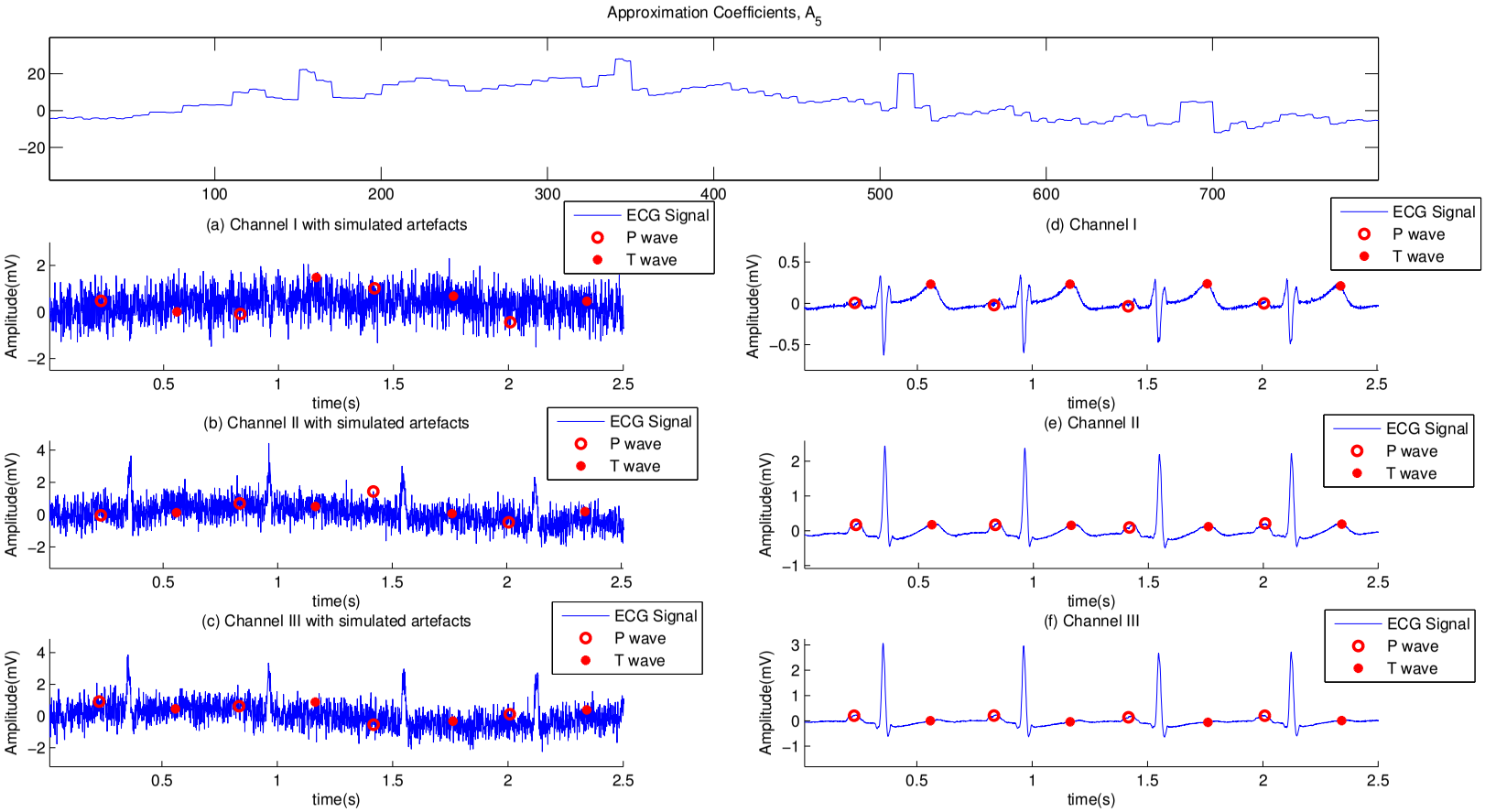

Figure 5.9: Top: Reshaped A_5 coefficients, (a)-(c):P and T wave detection on ECG signal with simulated baseline wander and EMG noise at SNR 0dB, (d)-(e): Detected P and T wave instances juxtaposed onto the original, clean ECG signal

Chapter 6

Conclusion and Future Work

Electrocardiogram analysis provided the perfect platform for VPW-FRI and FRI to demonstrate the power and flexibility of the methods. The numerous features in ECG made it an easily understood model on how VPW-FRI could be used for compression and feature detection. Given that certain cardiac conditions or arrhythmias produce rather deterministic signals, this removes the need for machine learning and training based methods especially if these features within the ECG can be identified analytically as is done by VPW-FRI. Diagnoses are rule based, with rules developed by researchers and clinicians. One way in which machine learning could be useful is in determining new rules and hidden relationships between different events in an ECG. This would be a more disruptive approach and is likely to be the direction of future work, especially in the fields of ECG and EEG analysis.

The hybrid models showed how parameters of different methods could easily be passed into FRI for processing. Its ability to identify various kernels gives it flexibility in processing various types of data. This would be particularly useful to study especially since in [13], spline and wavelet kernels were explored. Denoising capabilities would be a big advantage to this hybrid system as demonstrated in Section 5.4.

Another application would be the extension of VPW-FRI to imaging. Only in bi-level images are there discontinuities at boundaries and often in imaging, softer boundaries are present. The variability in the VPW-FRI kernel allows for analysis of these softer boundaries.

Also, work on multimodal data would be a logical next step. In a hospital bedside setting, the patient is being monitored using a variety of signals. Automated identification of common features within these signals and forming groups of signals relevant to each other would be a topic of interest. This would allow for automatic identification of signals and common feature detection using a common annihilator style approach. In [29], a version of this method was used to detect noisy channels which do not contribute to the common annihilator in the calculation of the location parameters. The specific contributions can be seen and thus the channels which contain the relevant information can be identified, or conversely, the channels which are not useful could be identified too.

List of Publications

1. A. Nair, P. Marziliano, R. F. Quick, R. E. Crochiere and G. Baechler, "Multichannel ECG Analysis Using VPW-FRI", *10th International Conference on Sampling Theory and Applications*, Bremen, Germany, July 1-5, 2013

2. A. Nair and P. Marziliano, "Fetal Heart Rate Detection Using VPW-FRI", *In Proceedings of the International Conference on Acoustics, Speech and Signal Processing, ICASSP 2014*, Florence, Italy

3. A. Nair and P. Marziliano, "P and T Wave detection on Multichannel ECG Using FRI", *In Proceedings of Engineering in Medicine and Biology Conference (EMBC)*, Aug 2014, Chicago, USA

4. A. Nair and P. Marziliano, "Noisy Channel Detection Using The Common Annihilator With An Application To Electrocardiograms" , *ICASSP 2015, Brisbane, Australia*

Bibliography

[1] M. Vetterli, P. Marziliano and T. Blu, "Sampling Signals With Finite Rate of Innovation", *IEEE Transactions on Signal Processing*, vol. 50, no. 6, pp. 1417-1428, June 2002.

[2] R. F. Quick, R. E. Crochiere, J. H. Hong, A. Hormati and G. Baechler, "Application of FRI to Modeling of Electrocardiogram Signals", *IEEE International Conference on Engineering in Medicine and Biology 2012, San Diego, USA*, pp. 2909-2912, August 2012.

[3] G. Baechler, N. Freris, R. F. Quick and R. E. Crochiere, "Finite Rate of Innovation Based Modeling and Compression of ECG Signals", *Proc. IEEE Int. Conf. on Acoustic, Speech, and Signal Processing (ICASSP), Vancouver, Canada 2013.*

[4] A. Hormati and M. Vetterli, "Compressive Sampling of Multiple Sparse Signals Having Common Support Using Finite Rate of Innovation Principles", *IEEE Signal Processing Letters*, vol. 18, no. 5, May 2011

[5] J. Onativia, J. A. Uriguen and P.L. Dragotti, "Sequential Local FRI Sampling of Infinite Streams of Diracs", *Proc. IEEE Int. Conf. on Acoustic, Speech, and Signal Processing (ICASSP), Vancouver, Canada 2013.*

[6] Y. Hao, P. Marziliano, M. Vetterli, T. Blu, "Compression of ECG as a Signal with Finite Rate of Innovation", *27th IEEE International Conference on Engineering in Medicine and Biology*, pp. 7564-7567, January 2005

[7] I. Maravic and M. Vetterli, "Sampling and Reconstruction of Signals with Finite Rate of Innovation in the Presence Noise", *IEEE Transactions on Signal Processing*, vol.53, no.8, pp. 2788-2805, August 2005.

[8] T. Blu, P. L. Dragotti, M. Vetterli, P. Marziliano and L. Coulot, "Sparse Sampling of Signal Innovations", *IEEE Signal Processing Magazine*, vol. 25, no. 2, 2008.

[9] A. Nair, P. Marziliano, R. F. Quick, R. E. Crochiere and G. Baechler, "Multichannel ECG Analysis Using VPW-FRI", *10th International Conference on Sampling Theory and Applications*, Bremen, Germany, July 1-5, 2013

[10] J. A. Lipponen, M. P. Tarvainen, "Advanced Maternal ECG removal and Noise Reduction for Application of Fetal QRS Detection," *Computers in*

Cardiology 2013, Zaragoza 2013

[11] C. Haier, H. Dickhaus, "Fetal QRS Detection and RR Interval Measurement in Noninvasively Registered Abdominal ECG," *Computers in Cardiology 2013, Zaragoza 2013*

[12] M. Varanini, G. Tartarisco, L. Billeci, A. Marcerata, G. Pioggia, R. Balocchi, "Fetal QRS Detection and RR Interval Measurement in Noninvasively Registered Abdominal ECG," *Computers in Cardiology 2013, Zaragoza 2013*

[13] P. L. Dragotti, M. Vetterli and T. Blu, "Sampling Moments and Reconstructing Signals of Finite Rate of Innovation: Shannon meets Strang-Fix", *in IEEE Transactions on Signal Processing*, vol. 55, no. 5, pp. 1741-1757, May 2007.

[14] R. Tur, Y. . Eldar and Z. Friedman, "Innovation Rate Sampling of Pulse Streams with Application to Ultrasound Signals", *in IEEE Transactions on Signal Processing*, vol. 59, no. 4, April 2011.

[15] J. Pan and J. W. Tompkins, "A real time QRS detection algorithm", *IEEE Transactions on Biomedical Engineering* , vol. BME-32, pp. 230-236,1985.

[16] K. Freeman and A. Singh, "P wave detection of ambulatory ecg", *In Proceedings of the Annual International Conference of the IEEE Engineering in Medicine and Biology Society*, 1991. Vol.13, pages 647 648, Oct-3 Nov 1991.

[17] J.F. Kaiser, "On a simple algorithm to calculate the energy of a signal", *In International Conference on Acoustics, Speech, and Signal Processing*, pages 381 384 vol.1, April 1990.

[18] R. E. Klabunde,, "Cardiovascular Physiology Concepts", September 2012. http://www.cvphysiology.com/.

[19] Nian-Qiang Li and Zheng-Sheng Wang, "T-wave detection in electrocardiogram signal based on independent sub-band function" *In International Workshop on Intelligent Systems and Applications*, ISA 2009., pages 1 3, May 2009.

[20] N. Sivannarayana and D.C. Reddy, "Biorthogonal wavelet transforms for ECG parameters estimation" *Medical Engineering and Physics*, 21(3):167 174, 1999.

[21] T.H.C. Tat, Chen Xiang, and Lim Eng Thiam, "Physionet Challenge 2011: Improving the quality of electrocardiography data collected using

real time QRS-complex and T-wave detection" *In Computing in Cardiology*, 2011, pages 441 444, Sept. 2011.

[22] Xiankui Wan and Du Xu, "An ECG T waves detection scheme based on the compensatory criterion", *In 3rd International Conference on Biomedical Engineering and Informatics (BMEI)*, 2010, volume 2, pages 730 734, Oct. 2010.

[23] A. Nair and P. Marziliano, "P and T Wave detection on Multichannel ECG Using FRI", *In Proceedings of Engineering in Medicine and Biology Conference (EMBC)*, Aug 2014, Chicago, USA

[24] A. Nair and P. Marziliano, "Fetal Heart Rate Detection Using VPW-FRI", *In Proceedings of the International Conference on Acoustics, Speech and Signal Processing, ICASSP 2014*, Florence, Italy

[25] J.R. Cox, F.M. Nolle, H.A. Fozzard, and G.C. Oliver, AZTEC, a preprocessing program for real-time ECG rhythm analysis, IEEE Transactions on Biomedical Engineering, vol. BME-15, no. 2, pp. 128129, apr. 1968

[26] Luisa F. Polania, Rafael E. Carrillo, Manuel Blanco Velasco, and Kenneth E. Barner, Compressed sensing based method for ECG compression, in IEEE International Conference on Acoustics, Speech, and Signal Processing, may 2011, pp. 761764.

[27] Robert A. Bruce, Frank W. Lovejoy, Raymond Pearson, Paul N. G. Yu, George B. Brothers, Tulio Velasquez, Normal respiratory and circulatory pathways of adaptation in exercise, J. Clin. Invest 28(6 Pt2), pp. 1423-1430, November 1949

[28] Goldberger AL, Amaral LAN, Glass L, Hausdorff JM, Ivanov PCh, Mark RG, Mietus JE, Moody GB, Peng C-K, Stanley HE. PhysioBank, PhysioToolkit, and PhysioNet: Components of a New Research Resource for Complex Physiologic Signals. Circulation 101(23):e215-e220 [Circulation Electronic Pages; http://circ.ahajournals.org/cgi/content/full/101/23/e215]; 2000 (June 13).

[29] A. Nair and P. Marziliano, "Noisy Channel Detection Using The Common Annihilator With An Application To Electrocardiograms" , *ICASSP 2015, Brisbane, Australia*